

STUDY OF THE RADIATION AND
CONVECTION ENVIRONMENT OF
THE SATURN V

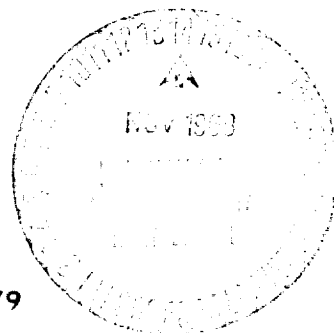
SUMMARY REPORT
CONTRACT NAS 8-11350

(NASA-CR-102469) STUDY OF THE
RADIATION AND CONVECTION
ENVIRONMENT OF THE SATURN 5 Summary
Report, Jul. 1965 - Oct. 1966
(Hayes International Corp.) 72 p

N94-71379

Unclass

Z9/20 0205093



INTERNATIONAL CORPORATION
BIRMINGHAM, ALABAMA

HAYES INTERNATIONAL CORPORATION

STUDY OF THE RADIATION AND
CONVECTION ENVIRONMENT OF
THE SATURN V

SUMMARY REPORT

For the Period July 1965 thru October 1966

CONTRACT NAS 8-11350

HAYES INTERNATIONAL CORPORATION

Birmingham, Alabama

ENGINEERING REPORT NO. 1333

October 31, 1966

by

John E. Reardon	H. J. Laney
Dr. Gordon B. McKay	Mohan Delwadia

ABSTRACT

This report presents a summary of the results of an experimental and analytical study of problems associated with rocket vehicle base heating. Radiation measurements of rocket exhaust plumes were made during sea level firings of a J-2 engine and a model rocket and during simulated altitude tests of S-II ullage motors and Centaur retro-rockets. The analytical portion of the study included modification and optimization of an exhaust plume radiation program, comparison of predicted and measured exhaust plume radiation, analysis of the S-II stage base heating model test results, and development of computer programs to size flow metering nozzles for base heating models.

TABLE OF CONTENTS

1.0	INTRODUCTION
2.0	RADIATION MEASUREMENTS
2.1	S-II Ullage Motor
2.2	Centaur Retro-rockets
2.3	J-2 Engine Static Firing
2.4	Model Rocket Engine Measurements
3.0	ANALYSIS
3.1	Radiation Computer Program
3.1.1	Carbon Absorption Coefficients
3.1.2	Reduction of Computer Time
3.1.3	Ware Number Step Size
3.2	Radiation Comparisons
3.2.1	Short Duration Model Tests
3.2.2	J-2 Engine Seal Level Firing
3.3	Saturn S-II Base Environment
3.4	Model Flow Nozzle Analysis
4.0	RECOMMENDATIONS
5.0	REFERENCES

1.0 INTRODUCTION

In order to provide better definition of the base environment on rocket vehicles and the Saturn V vehicle in particular, a number of radiation measurements and analytical studies have been conducted under contract NAS 8-11350 for NASA/MSFC. The first portion of this contract, during which radiation measurements were made on the F-1 engine was reported in reference 1. This summary report covers the work performed from June 1, 1965 to October 31, 1966.

During this period, radiation measurements were made on Saturn S-II ullage motors, centaur retro-rockets, model liquid propellant rockets, and J-2 engines. The analytical work included modification and optimization studies of the MSFC exhaust plume radiation program, comparison of predicted radiation with radiation measurements, analysis of the S-II base heating model test results and prediction of portions of the base environment, and development of computer programs to size flow metering nozzles for base heating models.

This report contains a review of the work performed with references to results which have been reported separately.

2.0 RADIATION MEASUREMENTS

Radiation measurements were made using both a Block BD-1A spectrometer and a Hayes FF-1 radiometer. The dates of the tests and instruments used are summarized in Table 2-1. In addition to the tests listed, several tests were attempted in which engine or instrumentation difficulties prevented successful measurements. These tests included an instrument failure on a F-1 engine test and engine failures on a J-2 engine and model engine tests. Results of each measurement are presented in the following sections.

TABLE 2.1

Summary of Radiation Measurements

<u>Rocket</u>	<u>Date</u>	<u>Location</u>	<u>Instrument</u>	<u>Remarks</u>
<u>S-II Ullage Motor Program</u>				
S-II Ullage	6/28/65	OAL	FF-1	Simulated altitude firing into a diffuser
	6/30/65	OAL	FF-1	
	8/27/65	AEDC	FF-1	Simulated altitude firing with free plume expansion
	8/28/65	AEDC	FF-1	
	5/19/66	OAL	BD-1A	Simulated altitude firing into a diffuser
<u>Centaur Retro Rocket Program</u>				
TX-3	4/6/66	MSFC Cell 112	FF-1	Simulated altitude firings at approximately 120,000 feet.
Arcocel 268	4/29/66			
RPI, 13%	5/6/66			
TX-3	5/13/66			
UTX7757	5/20/66			
RPI, 2% A1	5/26/66			
<u>J-2 Engine Program</u>				
J-2	3/1/66	MSFC	BD-1A	Static test stand measurements
J-2	4/7/66			
<u>Model Rocket Engine Measurements</u>				
Model J-2	6/4/66	MSFC	FF-1	Sea level tests

2.1 S-II Ullage Motor

Measurements of the plume radiation from the S-II ullage motor were made during three separate test series at OAL (Daingerfield, Texas) and AEDC (Tullahoma, Tenn.).

Characteristics of the S-II ullage motor are listed in Table 2.2, and details of the test results are described below.

TABLE 2.2

S-II Ullage Motor Characteristics

Approximate Chamber press. -psia	1000
Exit diameter - inches	12
Throat diameter - inches	4.2
Area ratio	8
Approximate thrust - lbf.	23,000
Nozzle half angle-deg.	12
Propellant	NH ₄ ClO ₄ (82%), Al (4%), "Flexdyne" binder (12%), ballistic modifier (2%)

2.1.1 OAL Radiometer Measurements

Radiometric measurements were made on S-II ullage motors at Ordnance Aerophysics Laboratory (OAL), Daingerfield, Texas on June 28, and June 30, 1965. The radiant emittance of two S-II motors was measured with the motors operating at both environmental temperature limits and at a simulated altitude of 140,000 feet.

The experimental setup is illustrated in Figures 2.1 and 2.2. A viewing port and an alignment port were installed in the diffuser. For pre-firing alignment, a blackbody source was placed outside the diffuser a few inches from the alignment port and the FF-1 radiometer head, mounted 0.5 inches outside the viewing port, was sighted at the blackbody and positioned for maximum irradiance of the detector. This insured that the line-of-sight of the radiometer passed through the center line of the diffuser. The viewing port was sealed with a one-inch diameter, .065 inch thick sapphire window. After the initial setup, the alignment port was closed so that little disturbance of the flow pattern in the diffuser would result from placing the ports in the diffuser wall. Details of the port adapters are illustrated in Figure 2.3.

After each of the firings the sapphire window was coated sparsely on the inside with what appeared to be aluminum oxide. The outside surface of the sapphire was heavily coated with soot. It is believed that the soot was deposited during cutoff and the aluminum oxide was deposited through the firing duration. The sapphire window was cracked on the June 30 firing, probably because of thermal shock. Thermal shock may have been caused by the deposit of soot on the window. Since soot is a much better absorber than sapphire, a large temperature difference between the deposited soot and the window may have existed.

A 1273°K blackbody calibration source and both ullage motor firings were all viewed through the sapphire window. This allowed data reduction without

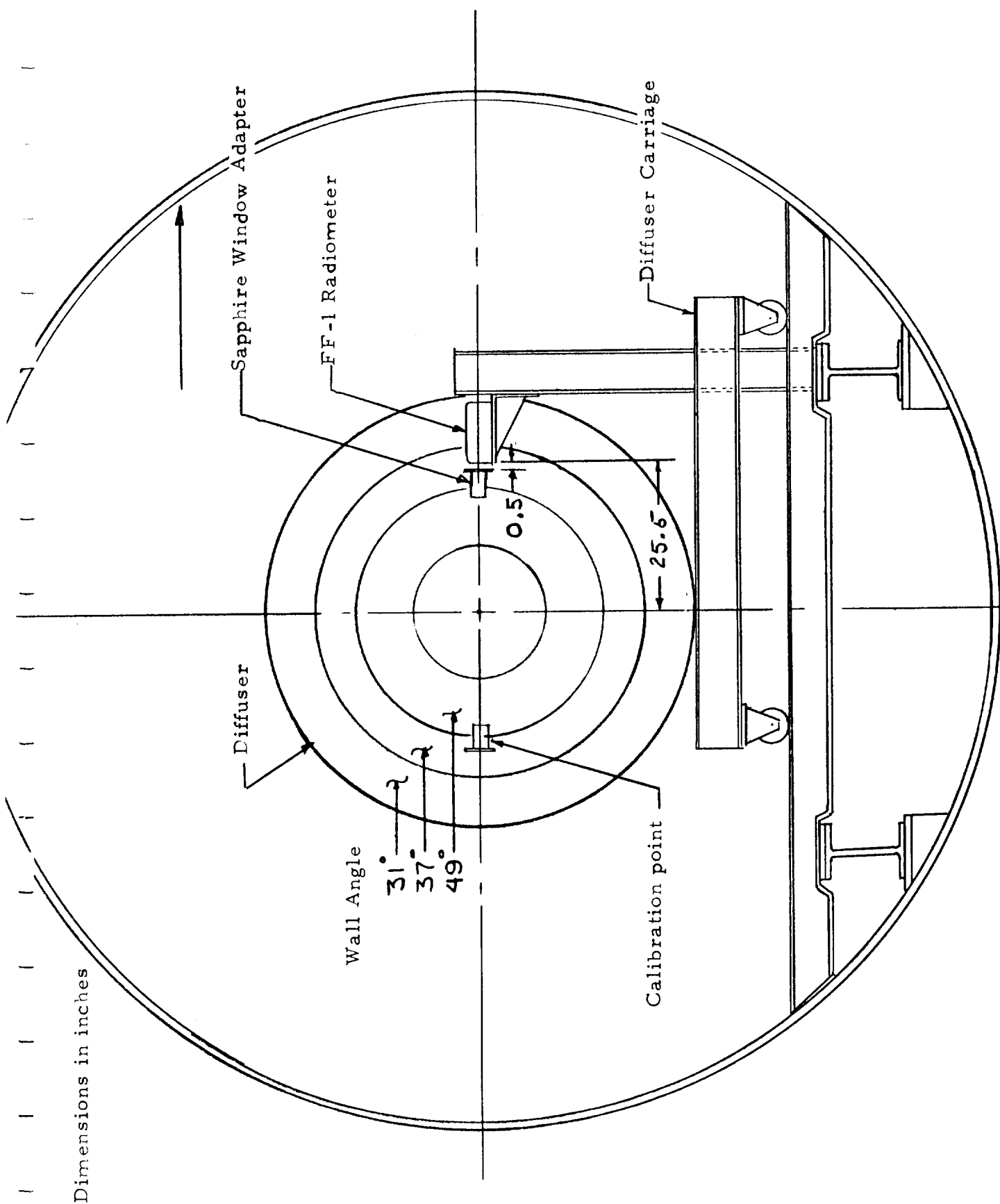


FIGURE 2.1 - FF-1 Radiometer Position - S-II ullage motor firings

All dimensions in inches.

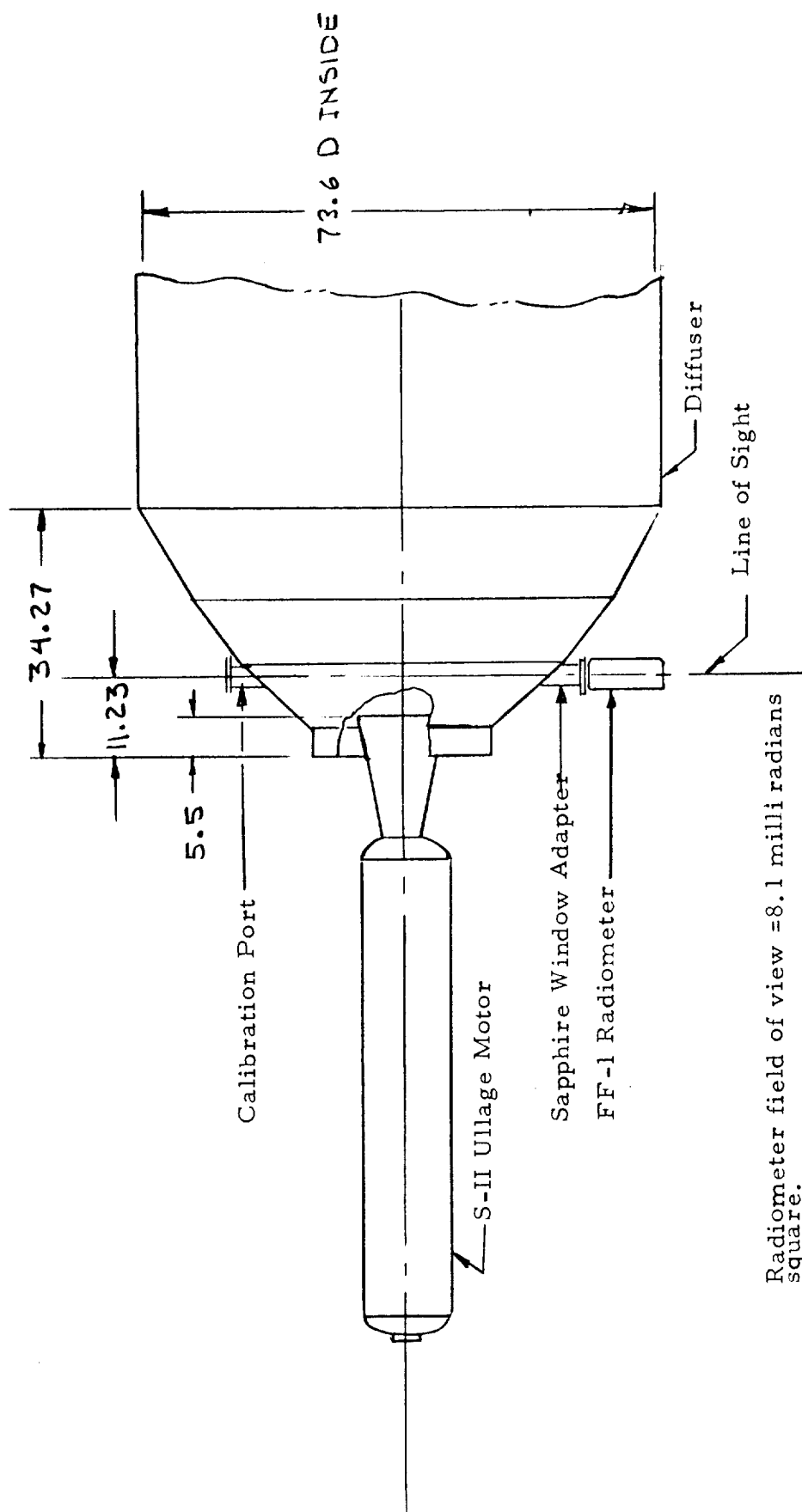


FIGURE 2.2 - Plan view - Radiometer installation

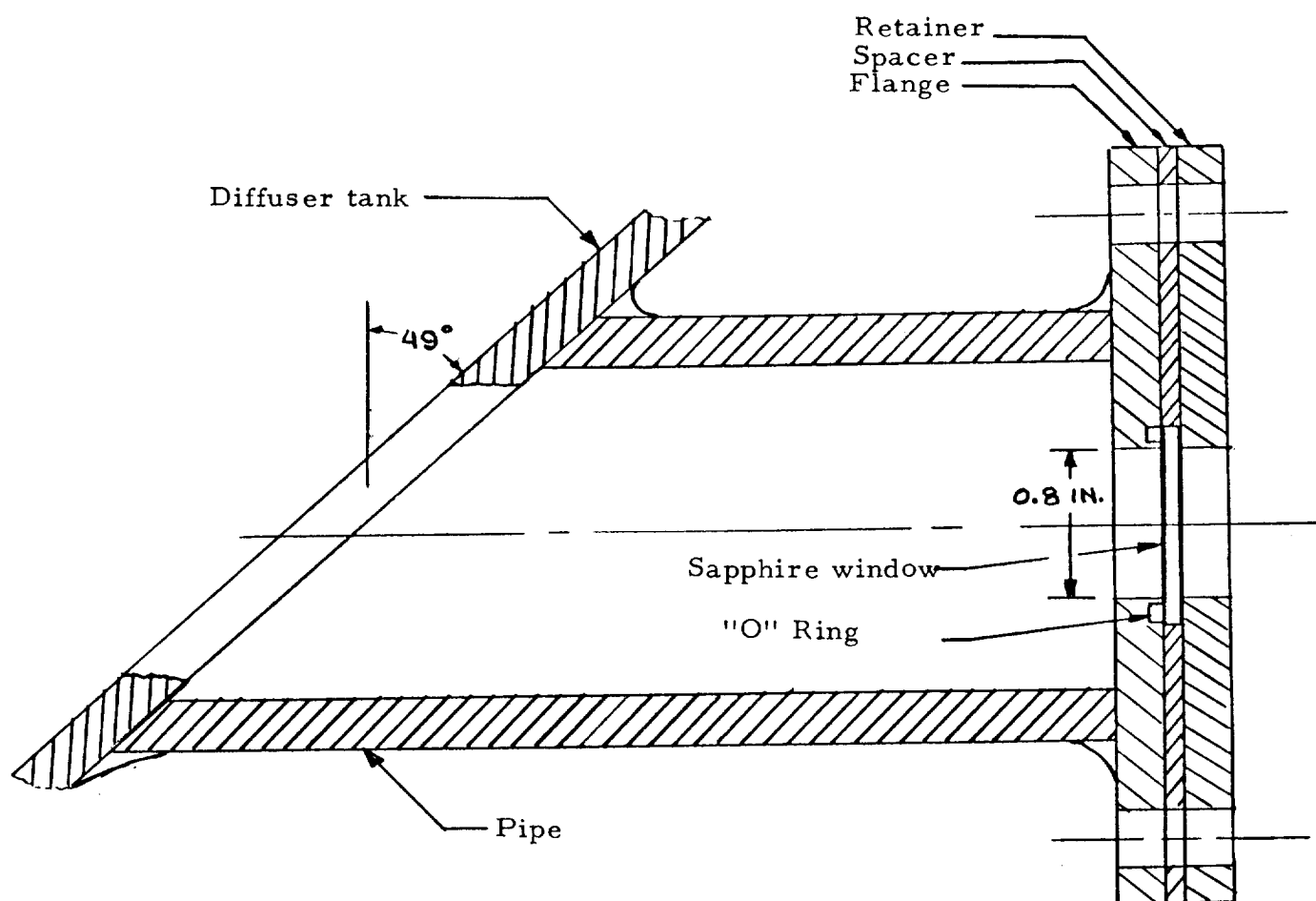


FIGURE 2.3 - Adapter for sapphire window

regard for the sapphire transmission characteristics because the transmission curve along the spectral region measured is relatively flat as is shown in Figure 2.4.

Data were reduced using the relation

$$W_E = W_S \frac{D_E}{D_S} \cdot \frac{B_S}{B_E} \cdot \frac{A_E}{A_S}$$

where

W = Radiant Emittance

D = % Deflection

B = Detector Bias Setting

A = Attenuator Setting

E = Emitter under test

S = Reference blackbody source

The results of the ullage motor firings are shown in Figure 2.5, but the fact that the sapphire window was coated after each test makes the absolute level of the data doubtful. Therefore, the higher indicated radiance levels measured later at AEDC are considered to be more reliable.

2.1.2 OAL Spectrometer Measurements

During May 1966 a Block Engineering Co. Model BD1-A spectrometer was used in an attempt to measure the spectral characteristics of S-II ullage motors during two firings. The experimental setup and alignment procedures were similar to those used during the radiometer measurements described previously except that the spectrometer was mounted in a small tank so that it would not be subjected

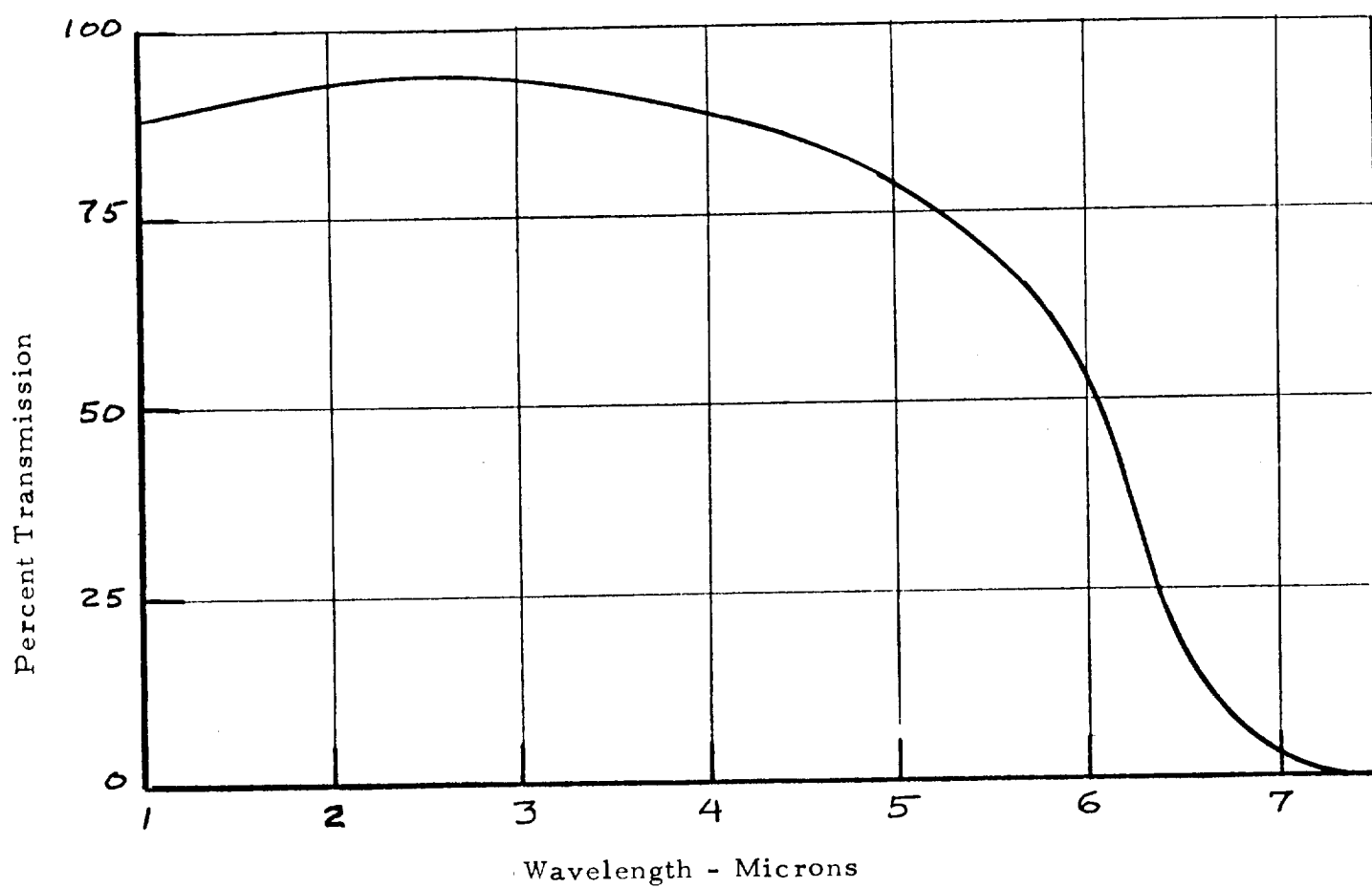


FIGURE 2.4 - Spectral Transmission of Sapphire (Al₂ O₃)

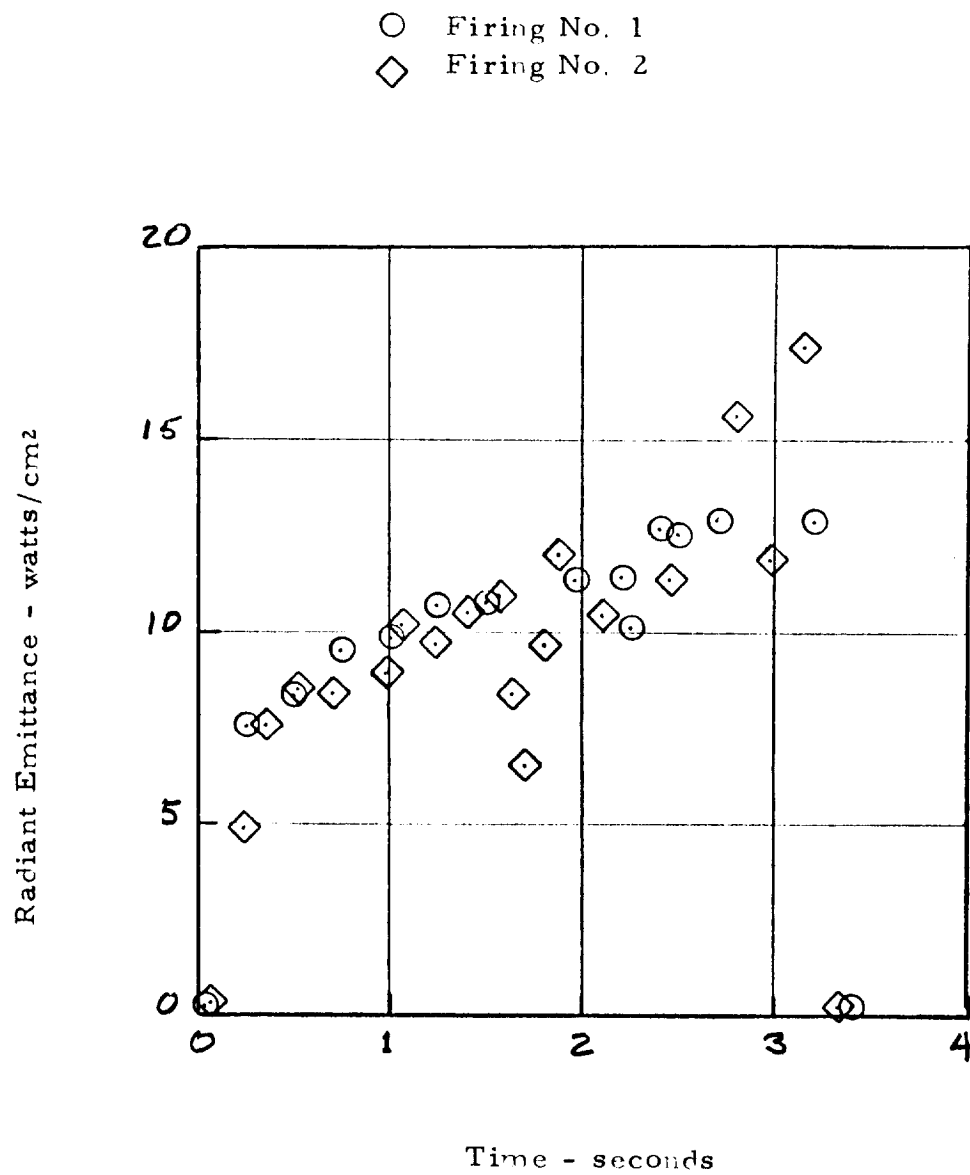


FIGURE 2.5 - Apparent Plume Radiant Emittance
on S-II Ullage Motor Firings at OAL.

to the simulated altitude pressure. This necessitated a second sapphire window, so that two (rather than one) sapphire windows were in the spectrometer line of sight.

The spectrometer response was checked by placing a source 28 inches from the spectrometer and inserting first one, then two, sapphire windows in the optical path. The two windows together attenuated the signal approximately 36%. Data reduction consisted of applying the calibration factors furnished by Block Engineering and dividing the resulting radiance by 0.64 to account for the window transmissivity. It is recommended that the results of this measurement be used only to evaluate relative spectral characteristics since there is some uncertainty concerning the spectrometer calibration and it has not been possible to obtain a recalibration. In addition, the window contamination problems described during the radiometer tests makes the accuracy of the measurements doubtful.

The results are presented for motor number 77 in Figure 2.6 and for motor number 78 in Figure 2.7.

2.1.3 AEDC Radiometer Measurements

Measurements of the radiant emittance of two S-II ullage motors were made at Arnold Engineering Development Center (AEDC), Tullahoma, Tennessee during August, 1965. The firings were made in a large chamber at simulated altitudes greater than 89,000 feet. These conditions allowed an unrestricted expansion of the plume, in contrast with previous S-II ullage motor measurements at OAL in which the plume was constrained by a diffuser.

Simulated altitude = 140,000 ft.
Motor preconditioned to 20°F

— Scan made at end of run
--- Scan made at middle of run
Scan speed $\approx 2/\text{sec}$.

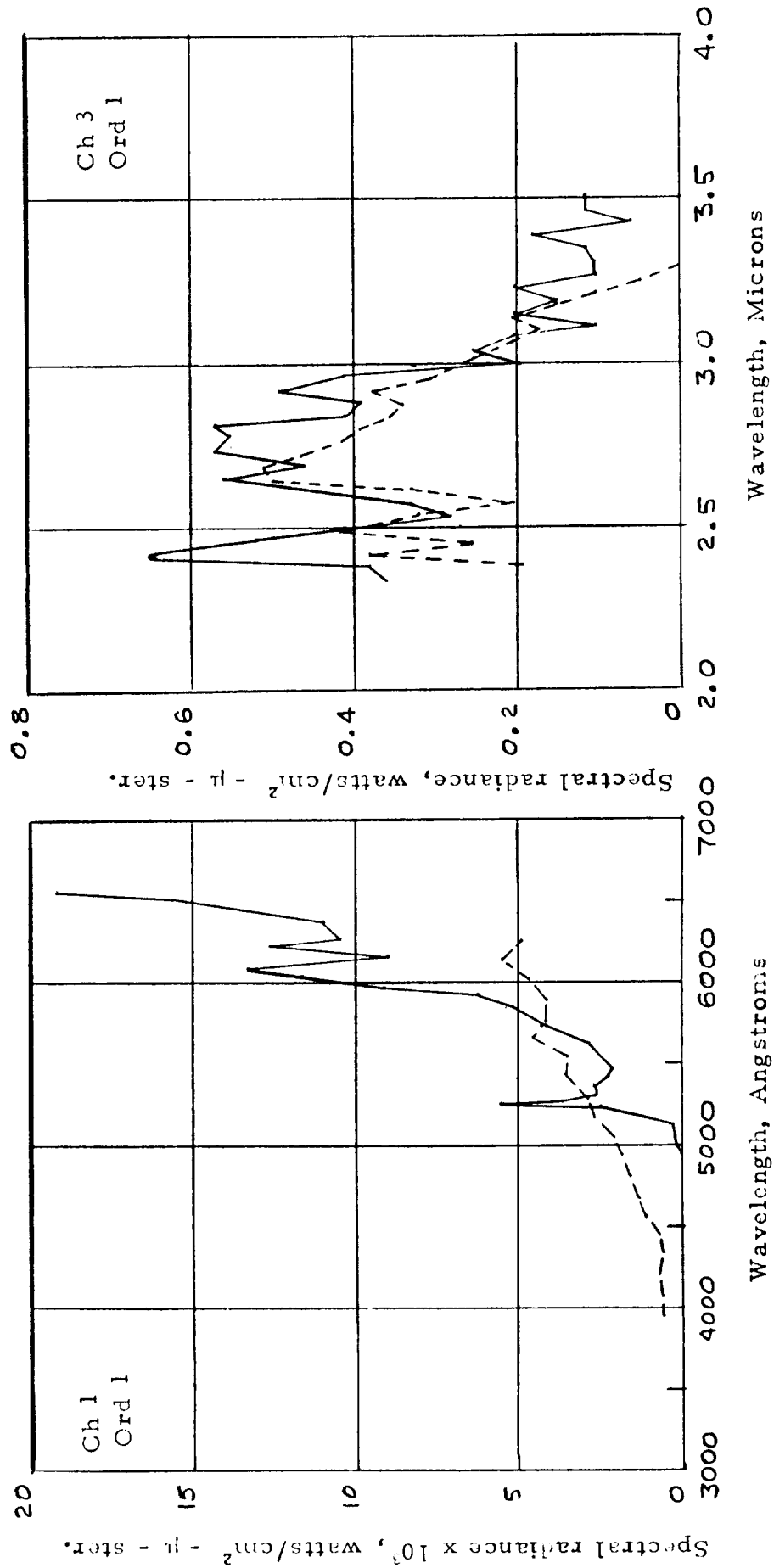


FIGURE 2.6 - Results of spectral measurements on S-II ullage motor no. 77

Simulated altitude = 140,000 ft.
Motor preconditioned at 125° F
Scan made at middle of run
Scan speed $\approx 2/\text{sec}$

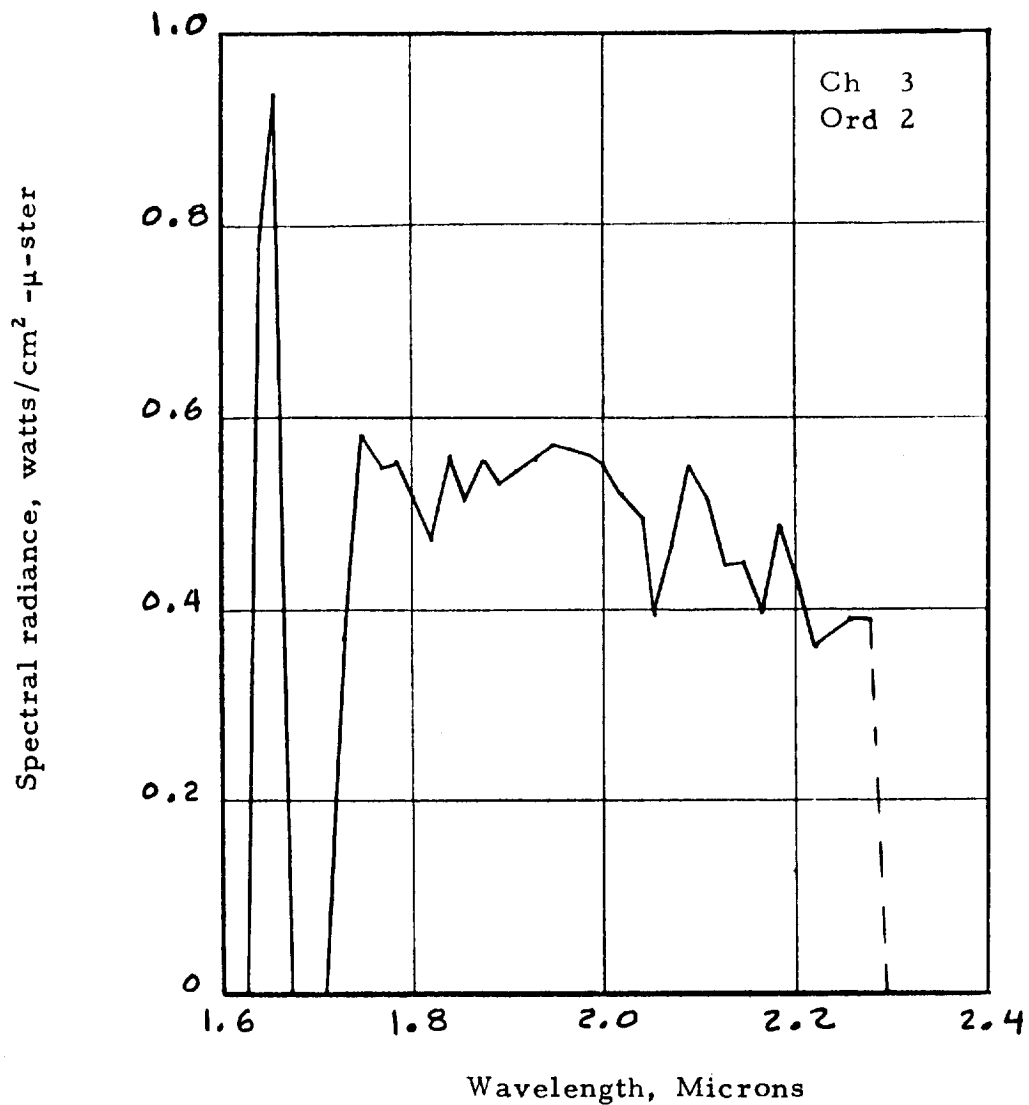


FIGURE 2.7 - Results of spectral measurements on S-II ullage motor No. 78.

During the S-II ullage motor firings, two Hayes-built infrared radiometers were utilized. One radiometer, Model FF-1, was located 6 inches above the nozzle exit plane and five feet off the nozzle center line and one radiometer, Model AH-1, was located approximately ten feet above the nozzle exit plane and twenty feet off the nozzle center line. A GN_2 purge (5 psig, 0.071 lb/sec maximum) was used on the FF-1 radiometer to aid in keeping aluminum particles and combustion products out of the radiometer. The AH-1 radiometer was placed in a sealed aluminum box maintained at atmospheric pressure and looked through a quartz window. The locations of the instruments are shown in Figure 2.8.

Calibration of the AH-1 radiometer was accomplished by viewing the reference blackbody source through the quartz window before and after each test. The Model FF-1 radiometer was calibrated before and after each test by viewing the reference blackbody source at 0.5" distance. There was a little obscuration of the quartz window after each firing, but calibration results indicated that this was negligible.

Data was reduced as described previously for the OAL radiometer measurements, and the results of the two firings are presented in Figure 2.9 for the FF-1 radiometer. The data obtained from the AH-1 radiometer were not completely satisfactory. However, the data indicated a peak radiant emittance in the range of 5.5 to 7.5 watts/cm².

The indicated radiant emittance of the two S-II motors used at AEDC was found to be considerably greater than that of two S-II motors tested in June, 1965 at the Ordnance Aerophysics Laboratory. As was noted in the description of the OAL tests, this difference was attributed to the adverse conditions under which

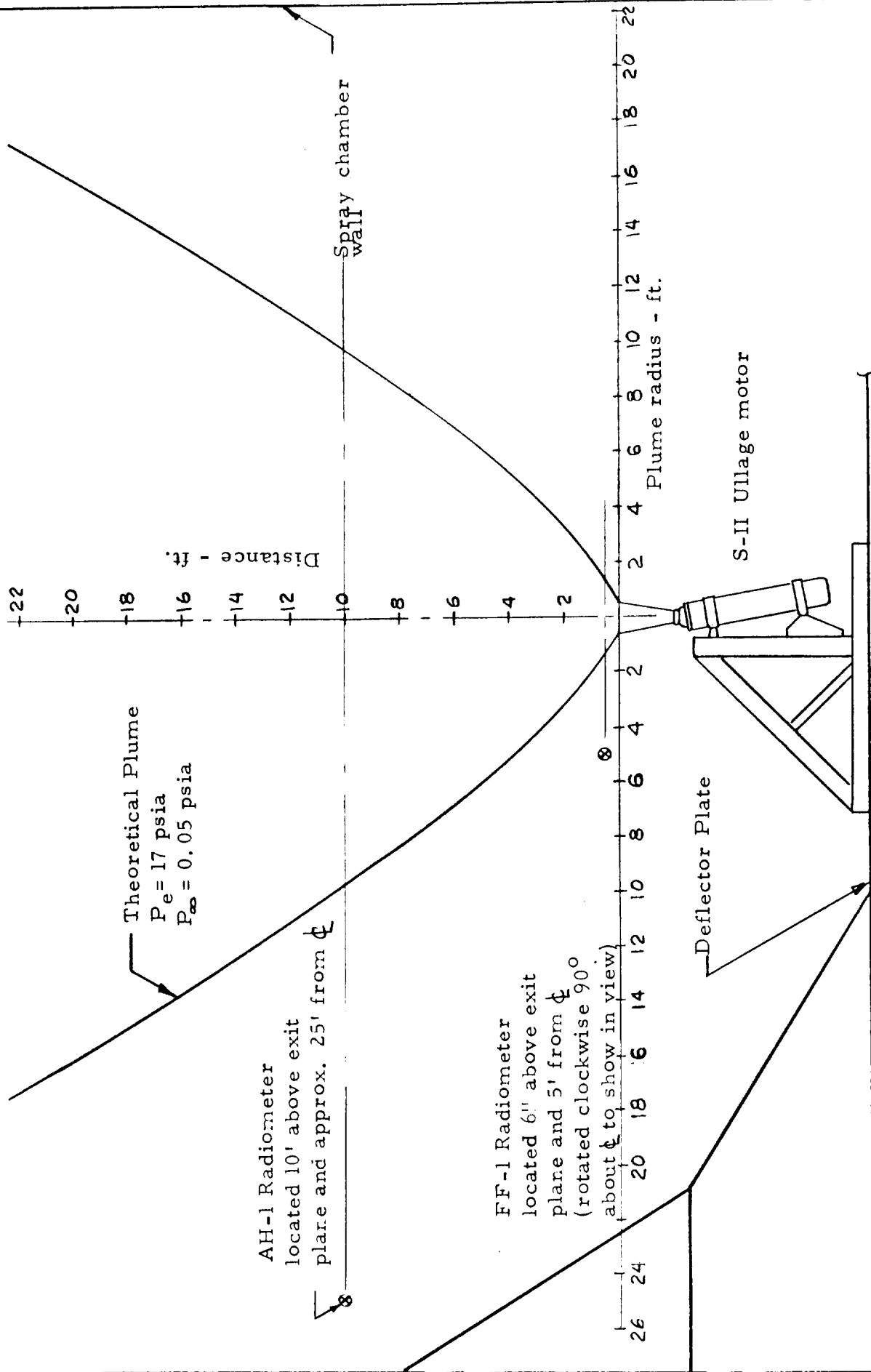


FIGURE 2.8 - Instrumentation locations for S-II ullage motor tests at AEDC

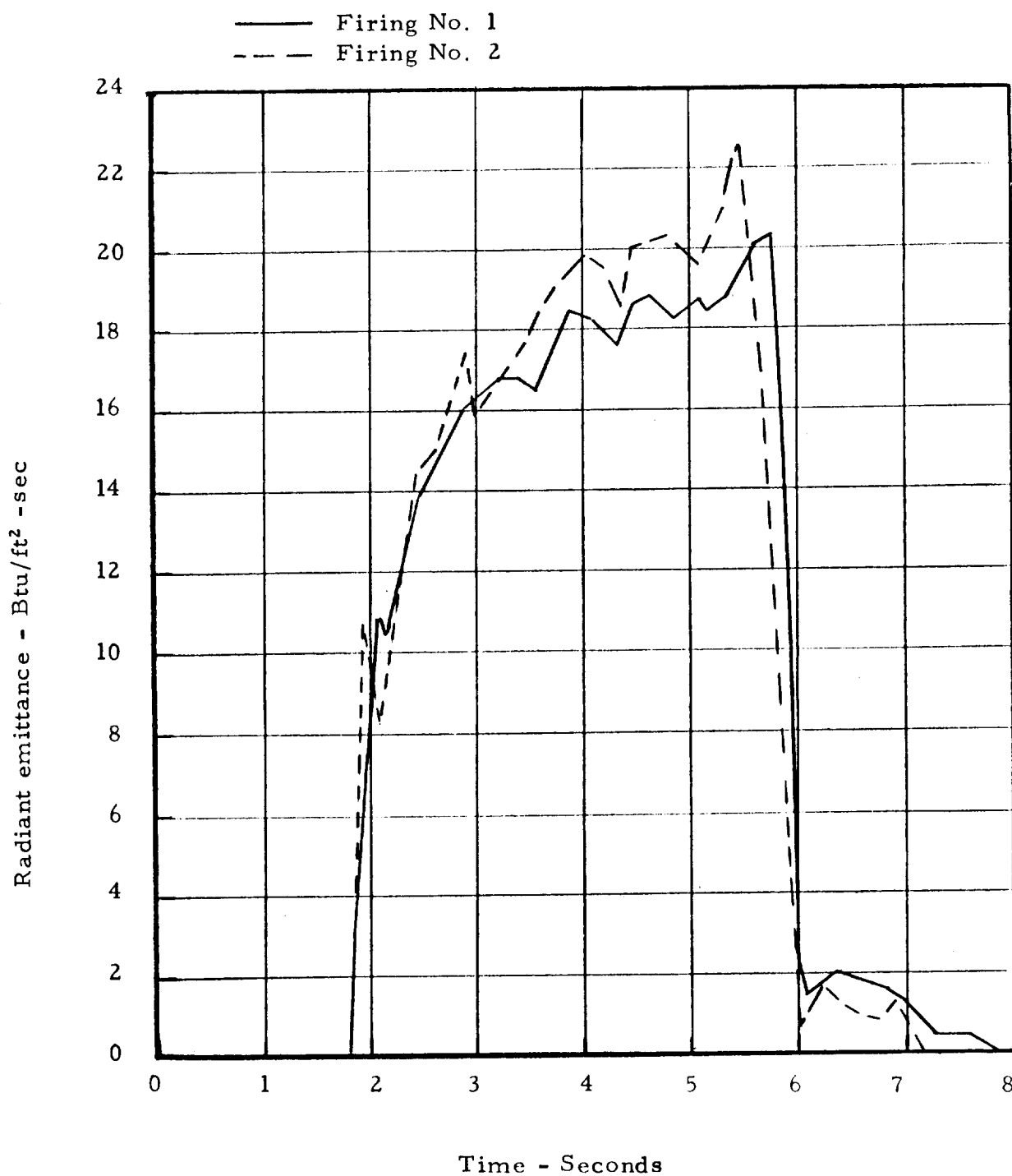


FIGURE 2.9 - Apparent Plume Radiant Emittance
on S-II Ullage Motor Firings

the OAL data was taken. In the OAL tests, the FF-1 radiometer looked at the plume through a sapphire window 5.75" downstream of the nozzle and 25.5" off the nozzle center line. During the firing the window became coated sparsely on the inside with what appeared to be aluminum oxide and was heavily coated on the outside with a material of soot-like appearance. These deposits contributed to the obscuration of radiation detected by the radiometer. At AEDC, no window was used on the FF-1 radiometer. A 5 psig flowing GN_2 purge was used to help prevent particles from entering the radiometer. The result of this effort was that there was no apparent obscuration and detection efficiency was greatly increased.

2.2 Centaur Retro-Rockets

A Hayes International Corporation Model FF-1 radiometer was used in measuring infrared radiation from each of a series of solid propellant Centaur retro-rocket engine firings of the "Solid Motor Contamination Test Program". The firings were conducted at simulated altitudes of approximately 120,000 ft. in Cell 112 at Vehicle Components and Sub-systems Branch test facilities of the MSFC test lab, Huntsville, Alabama. The motors tested were the Rocket Power, Inc. (RPI) 13% aluminum PBAA motor fired May 6, the Thiokol TX-3 polysulfide motor fired April 6 and May 13, the United Technology Center (UTC) UTX7757 motor fired May 20, the RPI 2% aluminum polysulfide motor fired May 26, and the Atlantic Research Corporation (ARC) Arcocel 268 nitrocellulose motor fired April 29.

The radiometer was mounted outside the plume 5 inches from the exit plane and 31" from the motor axis as shown in Figure 2.10.

Radiation heating data from the FF-1 radiometer, together with the applicable chamber pressure trace, are shown in Figures 2.11 thru 2.15. These data were taken from Reference 2.

2.3 J-2 Engine Static Firing

The spectral radiance of the J-2 engine was measured with the Block Engineering Co. BD-1A spectrometer during two static firings at MSFC. During the first test on 1 March 1966 (Test S-IVB-017) the spectrometer operated satisfactorily during the test with the exception of channel 4 (6μ to 12μ) which was excessively noisy. During the second test on 7 April 1966 (Test S-IVB-019) the drive gears on channels 1 and 3 (0.33μ to 0.66μ and 2.3μ to 4.6μ) stuck, so data was only obtained on channel 2 since channel 4 still had excessive noise.

The spectrometer was mounted 137.5 inches from the engine center line and aligned to view normal to the center line 7.5 inches downstream from the diffuser exit.

During both tests, a 5 inch long conical diffuser was attached to the J-2 exit. This diffuser is film cooled, and 16 to 20 lbm/sec of water is injected around the diffuser. During the first test (-017) the chamber pressure and mixture ratio of the engine were varied during the 400 second run time. For the first 280 seconds, the estimated nozzle stagnation pressure was 710 to 720 psia and the O/F ratio was 5.5. During the last 100 seconds, the nozzle

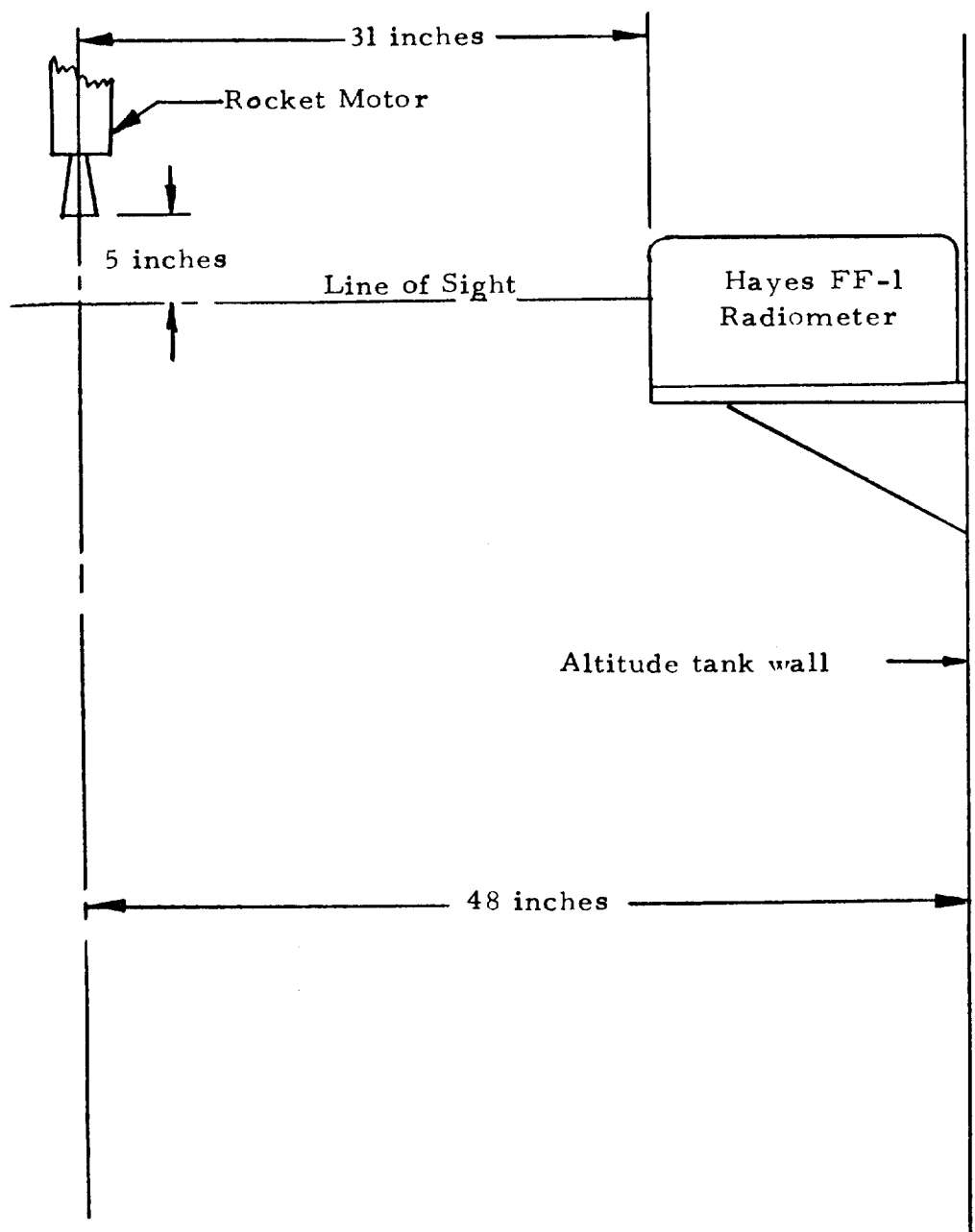
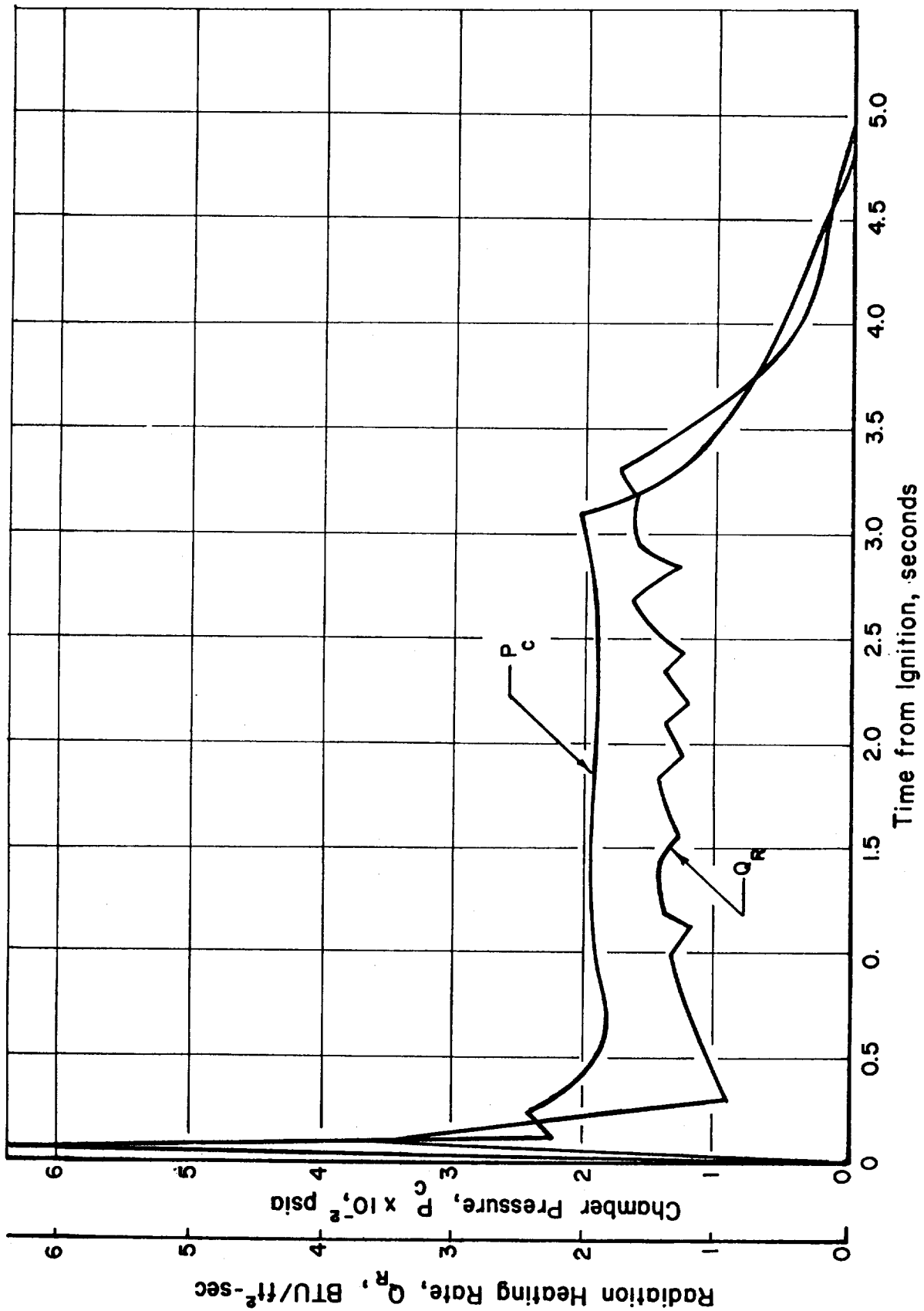


FIGURE 2.10 - Radiometer location for Centaur retro-rocket tests



RADIATION HEATING RATE AND CHAMBER PRESSURE VARIATION WITH
TIME FOR SECOND RPI-13%AL MOTOR FIRING

FIGURE 2.11

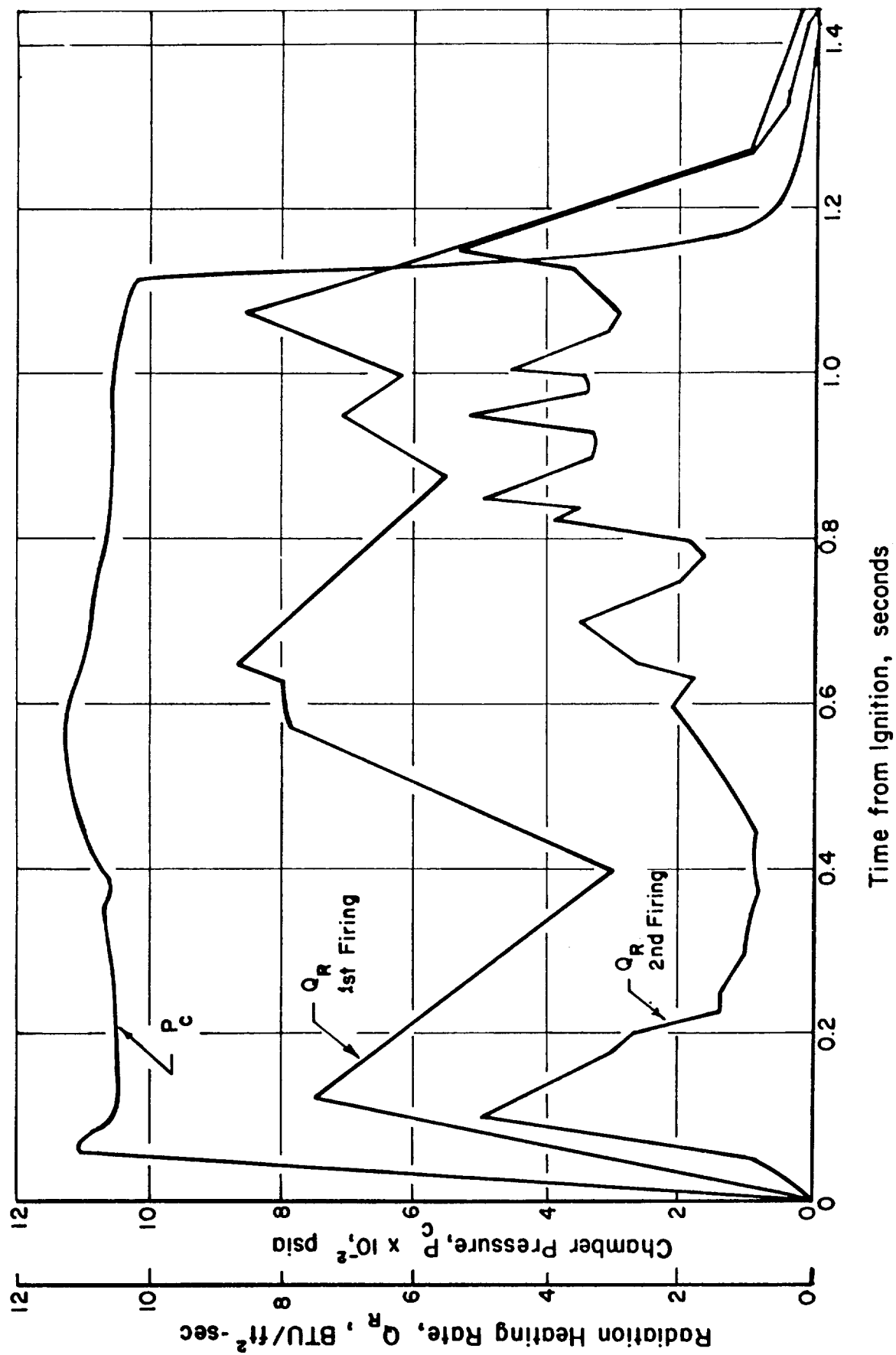
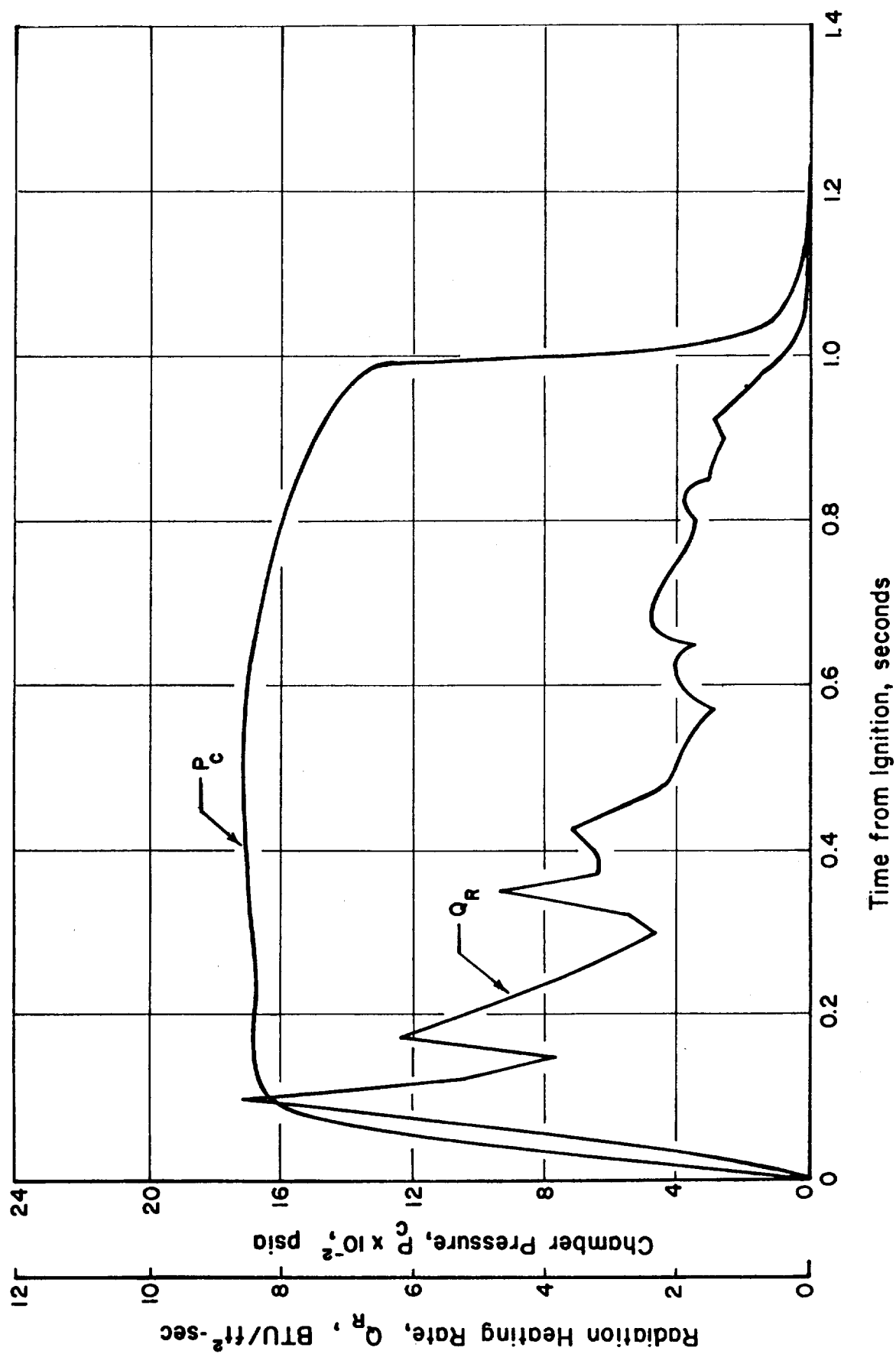


FIGURE 2.12

RADIATION HEATING RATE AND CHAMBER PRESSURE VARIATION WITH TIME
FOR TWO THIOKOL MOTOR FIRINGS



RADIATION HEATING RATE AND CHAMBER PRESSURE VARIATION WITH
TIME FOR SECOND UTC MOTOR FIRING

FIGURE 2.13

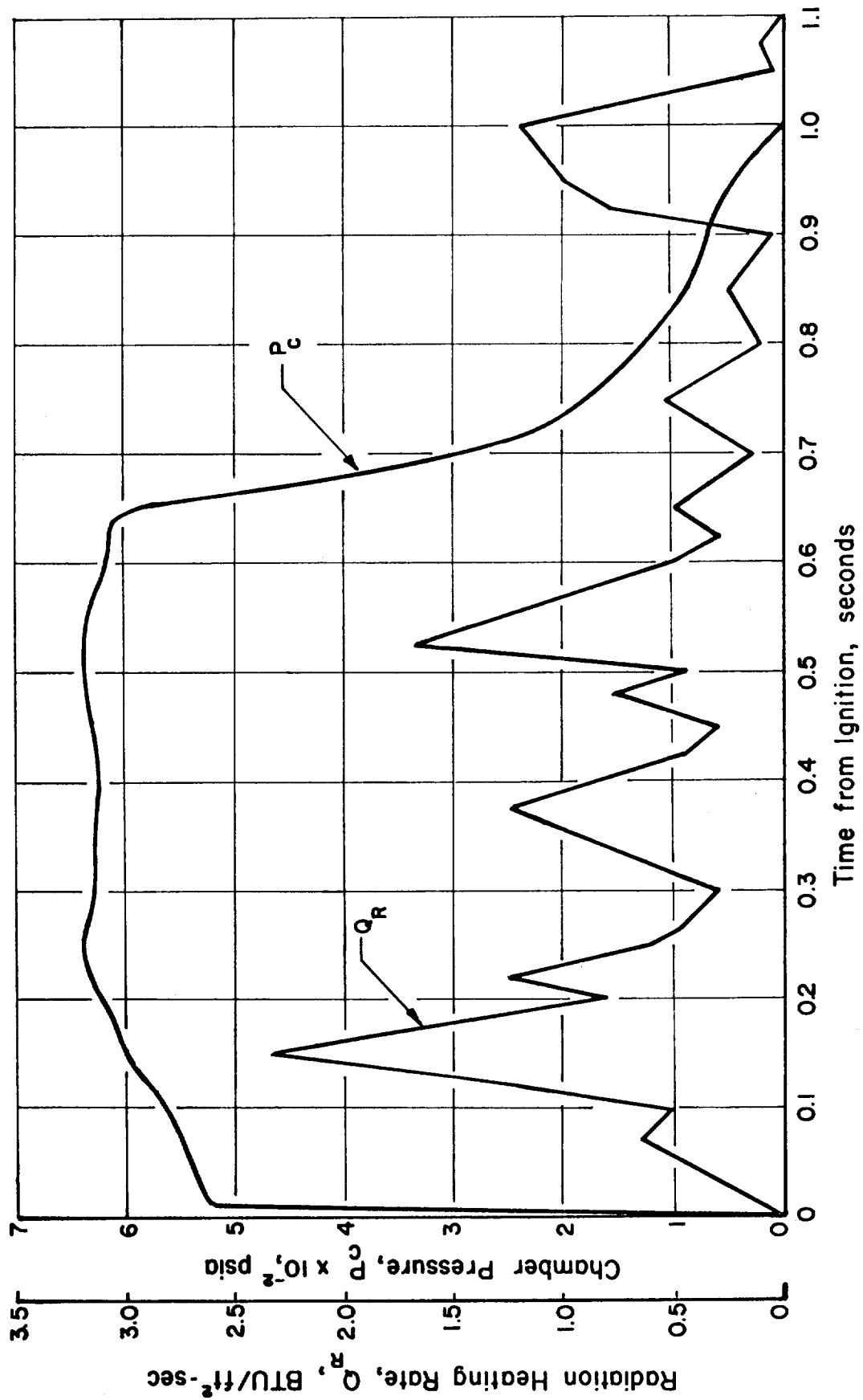
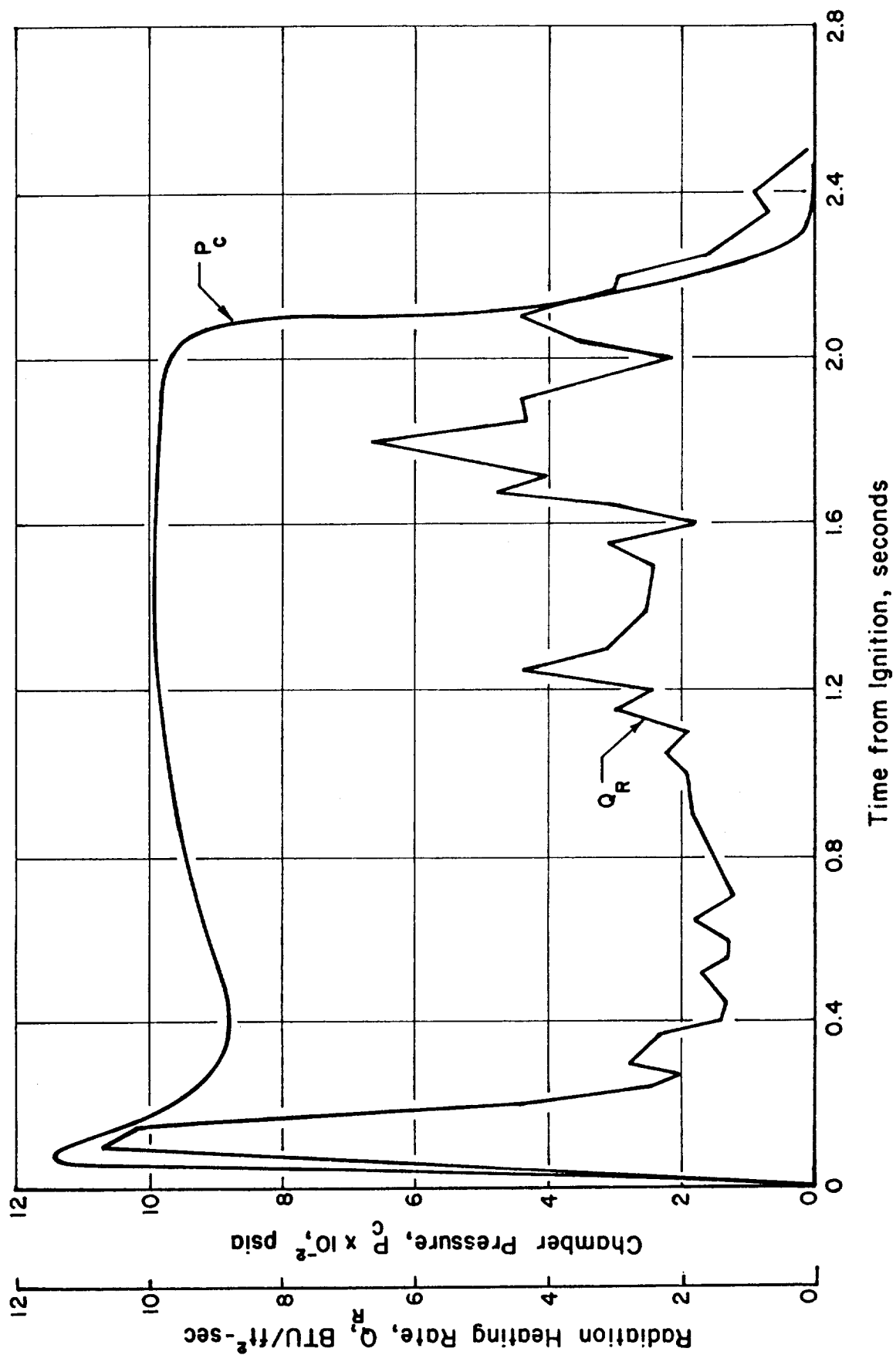


FIGURE 2.14

RADIATION HEATING RATE AND CHAMBER PRESSURE VARIATION WITH
TIME FOR SECOND RPI-2% AL MOTOR FIRING



RADIATION HEATING RATE AND CHAMBER PRESSURE VARIATION WITH
TIME FOR FIRST ARC MOTOR FIRING

FIGURE 2.15

stagnation pressure was 650 to 670 psia and the O/F ratio varied between approximately 5.0 and 5.06. The duration of the second test (-019) was only 200 seconds, and the estimated stagnation pressure and O/F ratio were constant at about 660 psia and 5.04. There were no significant changes in the measured radiation over the range of operating conditions and typical results are presented in Figure 2.16.

These data were reduced using pre-test calibration data furnished by Block Engineering and it has not been possible to get a post-test recalibration of the instrument.

2.4 Model Rocket Engine Measurement

A series of radiometer measurements were made on a model rocket engine at MSFC, Huntsville, Ala. The purpose of this test series was to validate previous measurement results obtained using radiation calorimeters mounted alongside the rocket plume.

Measurements were made with the Hayes Model FF-1 radiometer on tests 43 and 46 on June 4, 1965. Measurements were also attempted on tests 44 and 45 but the engine misfired.

The Model FF-1 total radiometer having a square field of view 8.1 milliradians per side was tripod-mounted 7.3 feet from the engine center line and aligned to view normal to the engine center line. The line of sight passed 9.75 inches aft of the engine exit in test 43 and 2.75 inches aft of the engine exit in test 46.

— Measurement at 91 sec. Nozzle stagnation press. ≈ 725 psia, C/F 5.48.
--- Measurement at 370 sec. Nozzle stagnation press. ≈ 655 psia, O/F 5.04.

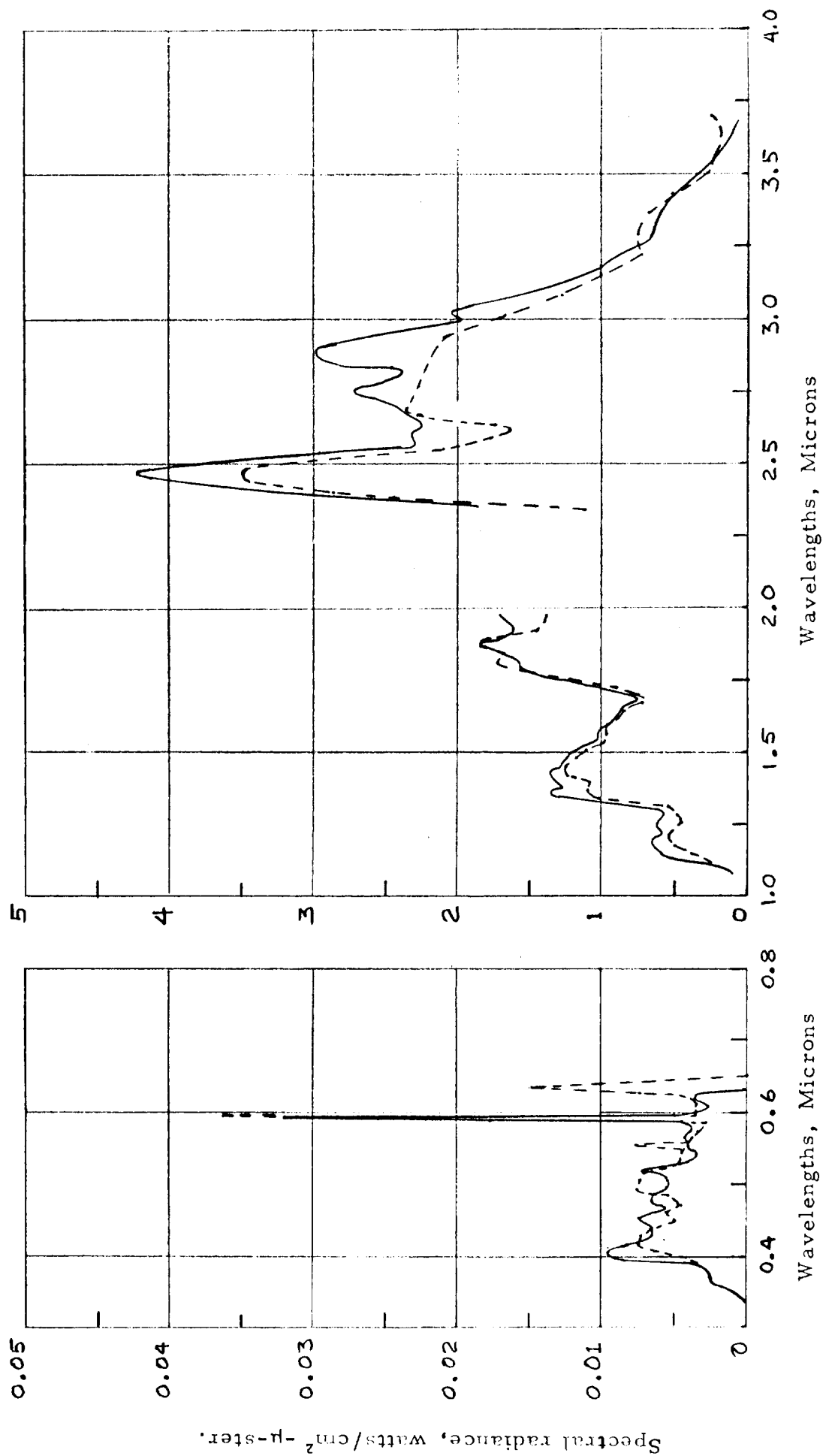


FIGURE 2.16 - Results of spectrometer measurements on a J-2 static test (S-IVB-017).

The radiometer was calibrated using a black body source at 1223°K before the runs and at 1273°K after the runs. The data was reduced as described previously in Section 2.1, and the results are presented in Table 2.3. The engine configuration used is shown in Figure 2.17.

All dimensions are in inches

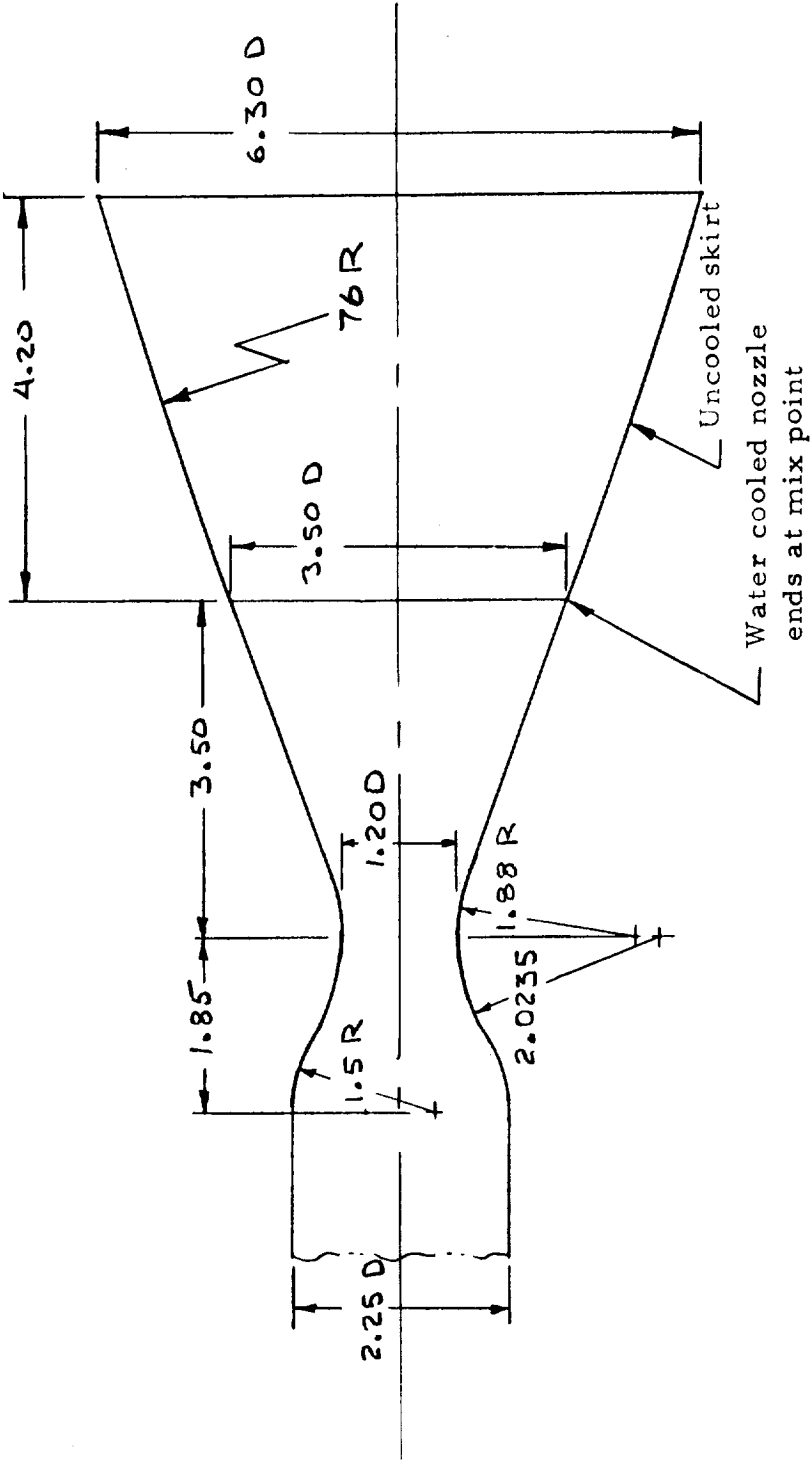


FIGURE 2.17 - Internal contours of model rocket engine

TABLE 2.3

Results of Model Engine Measurements

Test No.	43	46
Distance from engine exit - in.	9.75	2.75
Apparent plume emittance - watts/cm ²	8.64	9.38
Engine chamber pressure - psig	615	640
O/F ratio (Lox/GH ₂)	6.11	5.90

3.0 ANALYSIS

The analytical studies performed included the modification and optimization of the MSFC exhaust plume radiation computer program, comparison of predicted radiation with radiation measurements, analysis of the Saturn S-II stage base heating model test results and prediction of portions of the base environment and the development of computer programs to size flow metering nozzles for base heating models. Summaries of these studies are presented in the following sections.

3.1 Radiation Computer Program

A computer program for predicting the radiation from rocket exhaust plumes has been developed for MSFC through the contributions of several contractors. A description of the theoretical background of the computer program has been presented in Reference 3, and the latest detailed documentation of the program is available in Reference 4. However, the program is still in the process of development so final documentation is not yet available.

The radiation analysis uses band averaged absorption coefficients along with a modified Curtiss-Godson approximation to evaluate the radiation from multi-constituent inhomogeneous rocket exhaust plumes. The computation is performed using a spherical coordinate system with the origin at the point of interest. The line of sight or radius vector is s , and θ is the angle between s and the surface normal. The position of the projection of s in the plane of interest is defined by an angle ϕ . Using this coordinate system, the radiant flux per unit area at the point of interest is computed by the program using the summation

$$\dot{Q} / A = \sum_{\theta_i}^{\theta_f} \left[\sum_{\phi_i}^{\phi_f} \sum_{v_i}^{v_f} \sum_0^{s_f} - B_v^{\circ} (\tau_\ell - \tau_{\ell - \Delta \ell}) \right] \sin \theta \cos \theta \Delta \theta \Delta \phi \Delta v$$

where B_v° is the black body spectral radiance per unit wave number evaluated at the center of each 25 wave number interval.

The summation of the transmissivity begins with $\tau = 1$ and in subsequent increments uses

$$\tau_s = \exp - \sum_i \sum_0^s D_i$$

where the spectral optical path for each of the i radiating species, D_i , taking into account both doppler and collision broadening, is obtained at the center of each wave number interval using

$$\sum_0^s D_i = \sum_0^s F_i \left\{ 1 - \left[1 - \left(\frac{\sum_0^s D_{ic}}{\sum_0^s F_i} \right)^2 \right]^{-2} + \left[1 - \left(\frac{\sum_0^s D_{iD}}{\sum_0^s F_i} \right)^2 \right]^{-2} - 1 \right\}^{-\frac{1}{2}} \frac{1}{2}$$

where

$$F_i = \bar{k}_{i0} \rho_i \Delta s$$

the collision broadening is given by

$$\sum_0^s D_{ic} = \sum_0^s F_i \left[1 - \frac{\left(\sum_0^s F_i \right)^2}{\sum_0^s \frac{\gamma_{ic}}{d_i} F_i} \right]^{-\frac{1}{2}}$$

and the doppler broadening is obtained from

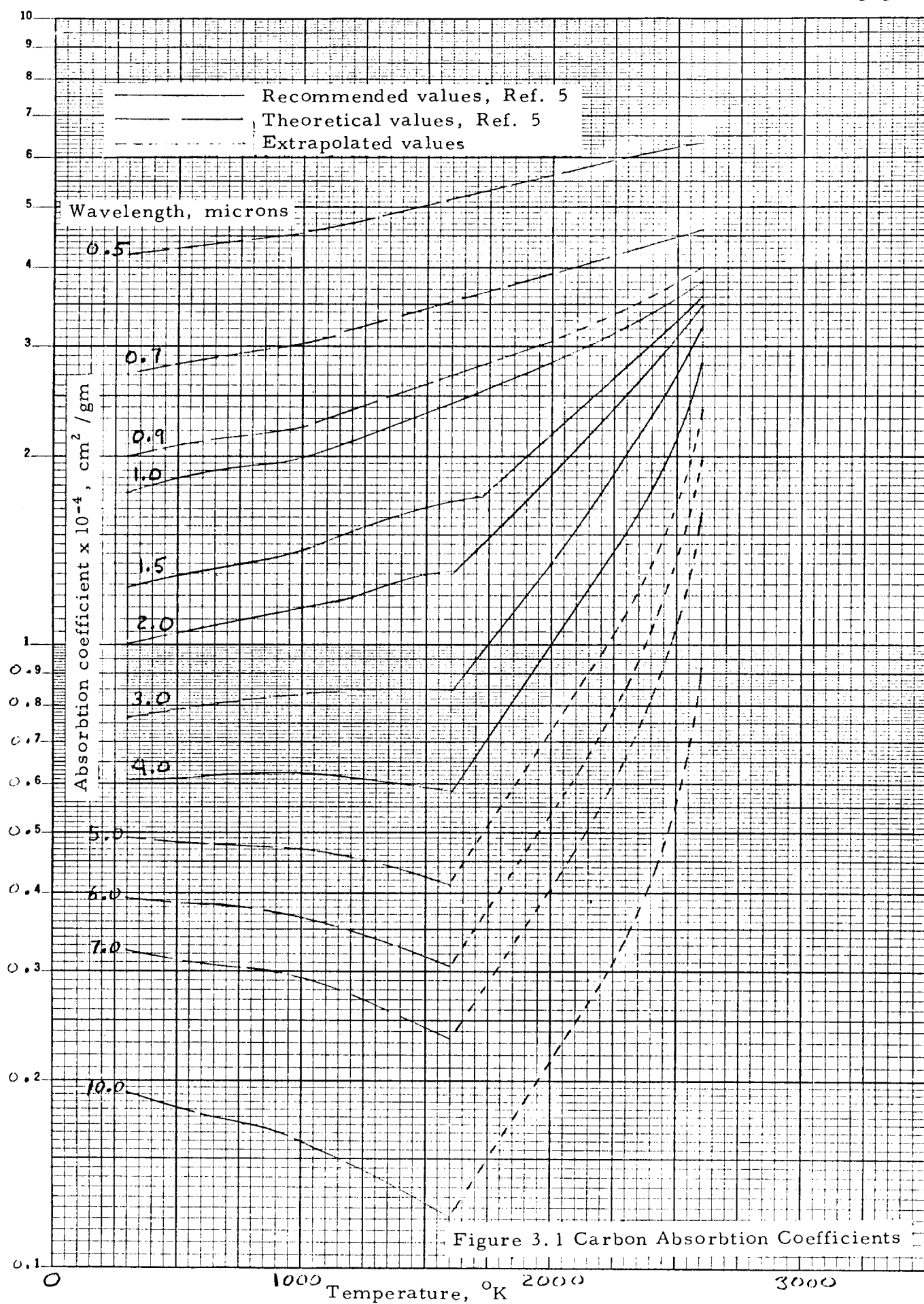
$$\sum_0^s D_{iD} = \frac{1.7 \sum_0^s \frac{\gamma_{id}}{d_i} F_i}{\sum_0^s F_i} \left\{ \ln \left[1 + \frac{0.589 \left(\sum_0^s F_i \right)^2}{\sum_0^s \frac{\gamma_{id}}{d_i} F_i} \right]^2 \right\}^{\frac{1}{2}}$$

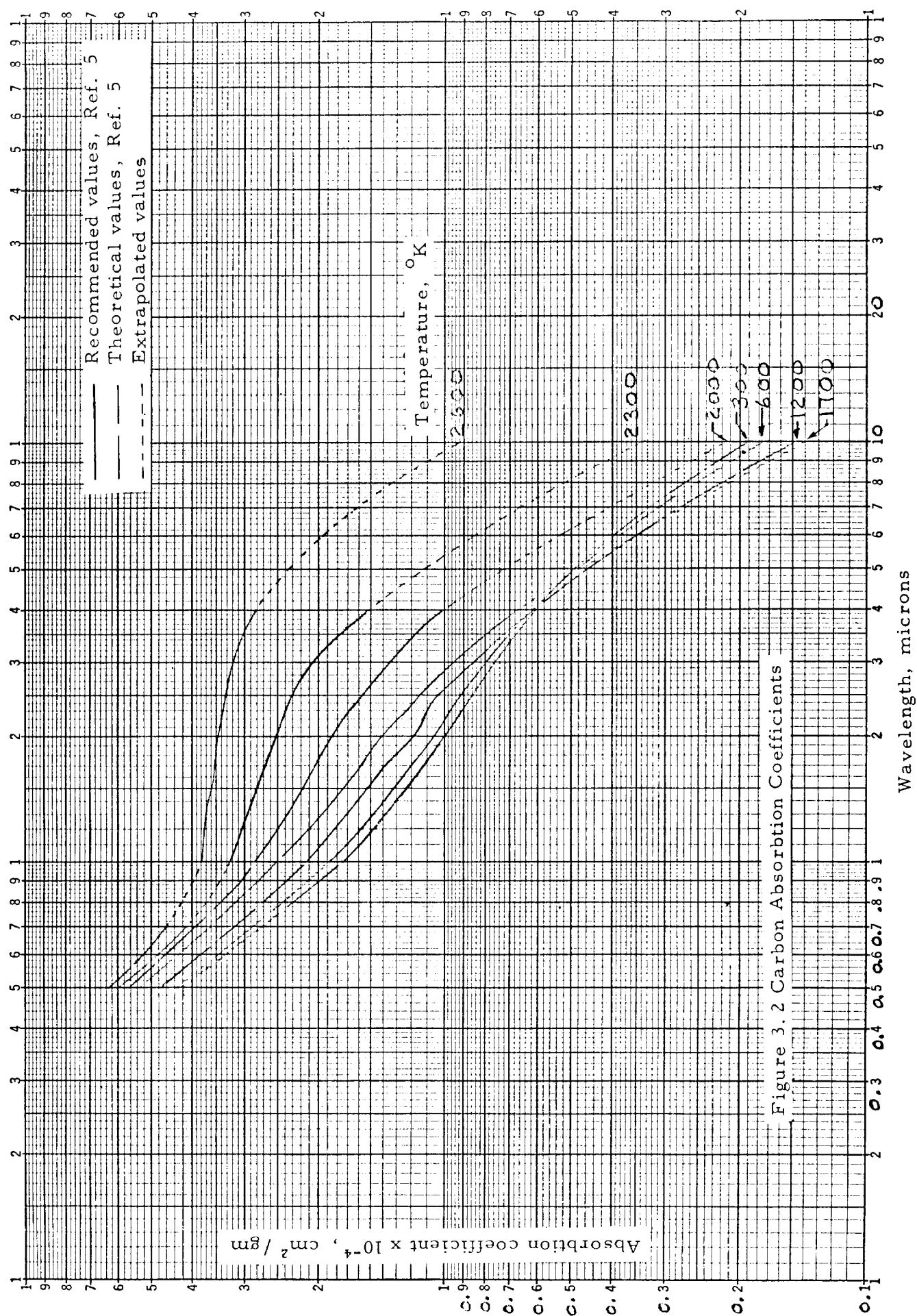
At the present time the computer program contains the necessary tabulated data and equations to compute radiation from H_2O , CO_2 , CO , and carbon particles. The studies performed under this contract included recommendations for the method of including the calculation of the carbon absorption coefficients, reduction of computer time by using larger integration step sizes with temperature limits as the controlling parameter, and a preliminary evaluation of effects of varying the wave number step size. The results of these studies will be summarized below.

3.1.1 Carbon Absorption Coefficients

Theoretical predictions and experimental measurements of absorption coefficients for clouds of small carbon particles were obtained from Reference 5. In the study reported in this reference, theoretical predictions of the absorption coefficients were made over the range of 0.5μ to 10μ and $150^\circ K$ to $3000^\circ K$. However, the experimental data indicated a deviation from the theoretical values for temperatures above $1600^\circ K$, and the final table of recommended absorption coefficients only covered a range of 1μ to 4μ as shown by the solid curves in Figure 3.1.

In order to extend the range of the data to other wavelengths a combination of methods were used. For the low temperatures and short wavelengths, where the theoretical predictions were in agreement with the experimental results over the range of wavelengths investigated, the theoretical predictions were used. For the high temperature and long wavelength regions, where the theoretical predictions are apparently invalid, the absorption coefficients were extrapolated following the trend noted in the experimental data. The resulting absorption coefficients





are shown in Figures 3.1 and 3.2.

In order to conserve computer storage it was desired that the carbon absorption coefficients be specified by curve fits rather than input as a table of values. Therefore, the absorption coefficients were fitted with 4th degree polynomials in wavenumber for the seven temperatures shown in Figure 3.2. The resulting coefficients are presented in Table 3.1, and the deviation of the curves from the desired values are listed in Table 3.2. Large errors are encountered at the long wavelengths, but due to the uncertainty in the absorption coefficient at these wavelengths and the small percentage of radiation at these wavelengths in most base heating problems, these errors are not considered to be excessive. It is also noted that the errors increase with increasing temperatures, but due to the uncertainty in the empirical data defining the absorption coefficients at high temperatures this is not considered a serious drawback. In Reference 5 it was estimated that the uncertainty in the empirical absorption coefficients at the highest temperatures may be as much as $\pm 50\%$.

3.1.2 Reduction of Computer Time

In using the exhaust gas radiation computer program for a single line of sight, the computer time may be on the order of a minute, but when integration over a complete hemisphere is required for several points in the base region, many hours may be required. Therefore, a study was made of possible techniques for reducing the computation time. No automated procedure could be proposed for varying the angular differentials $\Delta\theta$ and $\Delta\phi$, but some progress has been made in using a variable path length along the line of sight, Δs .

TABLE 3.1
Carbon Absorption Coefficient Curves

Temperature		A	B	C	D	E
$^{\circ}\text{K}$	$^{\circ}\text{R}$					
		$\times 10^4$	$\times 10^1$	$\times 10^{-3}$	$\times 10^{-7}$	$\times 10^{-12}$
300	540	-.13463853	.38710213	-.47055911	.35084341	-.79087507
600	1080	-.19909966	.42759743	-.50848071	.37144485	-.83813311
1200	2160	-.31886445	.48804827	-.52853813	.36589761	-.80385920
1700	3060	-.38870225	.53648682	-.50955662	.33136839	-.69866129
2000	3600	-.60273281	.86118469	-1.0340689	.64889548	-1.3474213
2300	4140	-.89695742	1.3577194	-1.8257443	1.1016709	-2.2102493
2600	4680	-.41368281	1.8460052	-2.9400371	1.9221795	-4.1482373

$$k_{\nu} = A + B\nu + C\nu^2 + D\nu^3 + E\nu^4$$

$$k_{\nu} = \text{Absorption coefficient, cm}^2 / \text{gm}$$

$$\nu = \text{Wave number, 1/cm}$$

TABLE 3.2

Errors in Carbon Absorption Coefficient

Wave- number 1/cm	Wave- length Micron	Percent Error						
		300°K	600°K	1200°K	1700°K	2000°K	2300°K	2600°K
1000	10.0	9.34	2.42	-17.3	-28.52	-24.58	-13.74	25.77
1429	7.0	2.89	3.44	2.17	5.30	7.43	7.12	3.60
1667	6.0	0.65	1.57	4.35	8.24	7.39	6.86	-1.91
2000	5.0	-2.42	0.23	3.45	5.38	3.53	4.71	-5.09
2500	4.0	-3.16	-1.33	2.28	2.11	.006	0.65	-6.10
2750	3.64	-1.91	-1.96	0.73	0.16	-1.70	-2.19	-5.52
3000	3.33	-1.22	-1.43	0.25	-0.47	-0.46	-3.07	-3.78
3333	3.0	-1.31	-1.45	-0.57	-0.89	-0.56	-2.90	-2.08
3636	2.75	-0.54	-0.32	-1.42	-1.39	-0.012	-2.89	-0.52
4000	2.5	0.60	-0.65	-2.79	-2.06	-0.11	-1.69	2.74
4444	2.25	0.91	0.74	-1.26	-1.36	-1.21	0.49	3.20
5000	2.0	1.36	0.90	1.44	-1.39	-0.81	2.24	3.73
5714	1.75	1.01	0.65	0.84	0.44	0.44	1.86	4.52
6667	1.5	0.65	1.27	0.08	2.14	0.88	2.42	2.83
8333	1.2	0.85	0.54	-0.68	1.15	-0.076	-0.063	-1.71
10000	1.0	-0.1	-0.62	1.01	-0.57	-0.001	-0.64	-2.12
11111	0.9	-1.78	-0.84	-0.31	-0.65	0.24	-1.68	-3.86
14286	0.7	0.63	0.38	-0.11	0.203	-0.18	0.78	2.61
20000	0.5	-0.035	-0.02	0.013	-0.006	0.019	-0.044	-0.20

Preliminary investigations of the allowable temperature change in an integration step were made using simulated gas fields with linear temperature distributions so that varying the integration step size, Δs , would vary the temperature step size. Tests were carried out on various H_2O radiation cases using both constant pressure and isentropically varying pressure in linear temperature fields. The results of these tests, presented in Figure 3.3, indicated that calculation accuracy of one per cent could be maintained with a temperature difference per integration step equal to five per cent of the mean temperature in the gas.

Since this method of increasing the speed of integration appeared promising, the program was modified to accept a desired temperature difference input. When this input is zero the integration is carried out with a constant Δs . When the input is not zero, the line of sight is searched using the input Δs increment until the temperature difference is equal to or slightly greater than the desired difference. Then, the transmissivity for the increment is computed using the average pressure, temperature, and mole fractions over the increment. Checks are included to stop the increment when the slope of the temperature changes and to back up one Δs step if the temperature difference exceeds the desired temperature difference by more than ten per cent.

The results of sample cases using this procedure with various temperature step sizes are presented in Figure 3.4. These results indicate that the time required for searching the slow field is very short compared with the time required for making the transmissivity calculations. Therefore, a

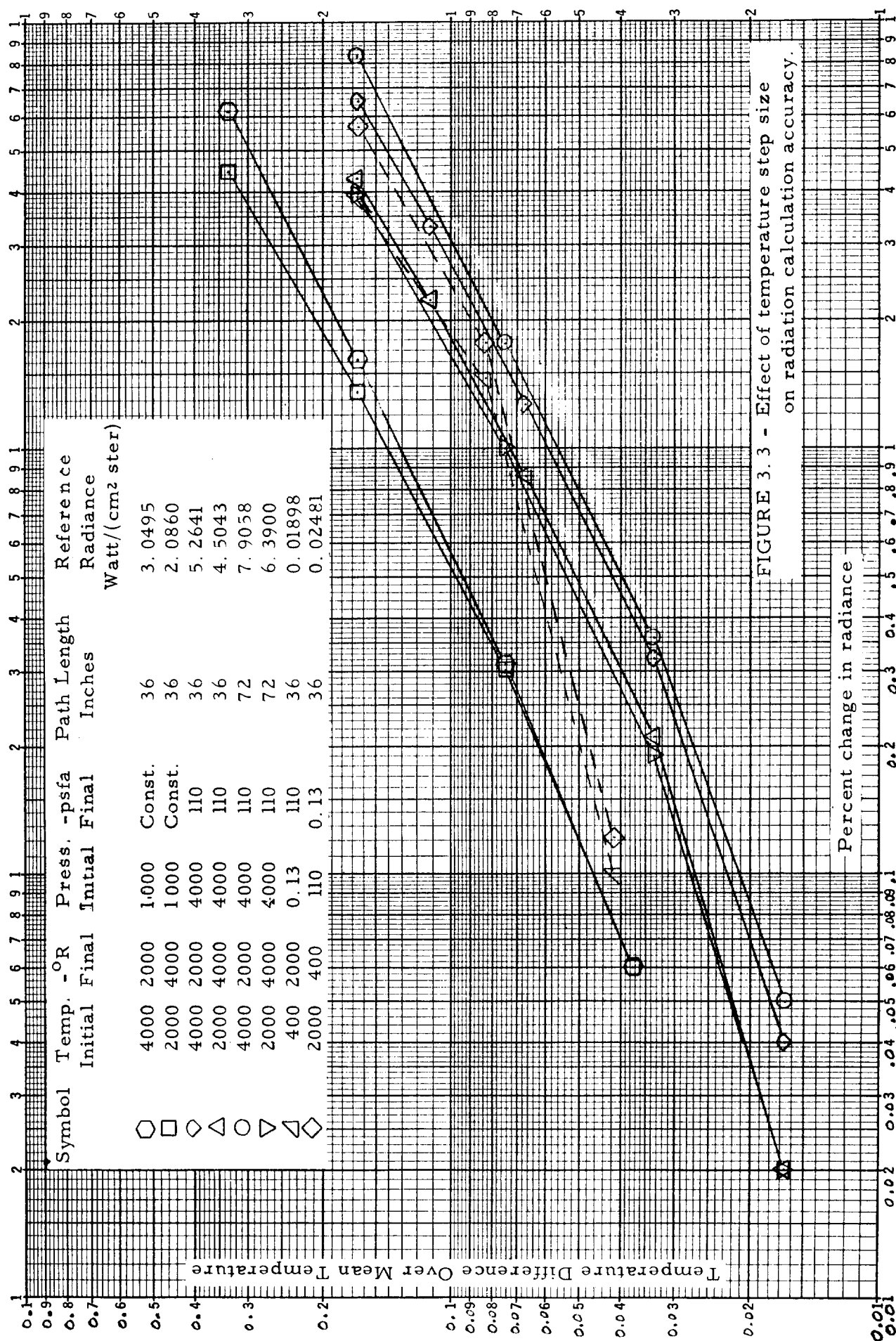


FIGURE 3.3 - Effect of temperature step size
on radiation calculation accuracy.

	Flow Field	Δs -in.	$\tau(o)$	$F(o)$, integrated over 1-5 μ
_____ Case 1	Fig. 3.7	0.05	80 sec.	0.546410 watts/cm ² -ster.
----- Case 2	Fig. 3.9	0.10	155 sec.	0.0506018 watts/cm ² -ster.

$\tau(o)$ = Computer run time with radiation integration step at each Δs step.

$F(o)$ = Computed flux with radiation integration step at each Δs step.

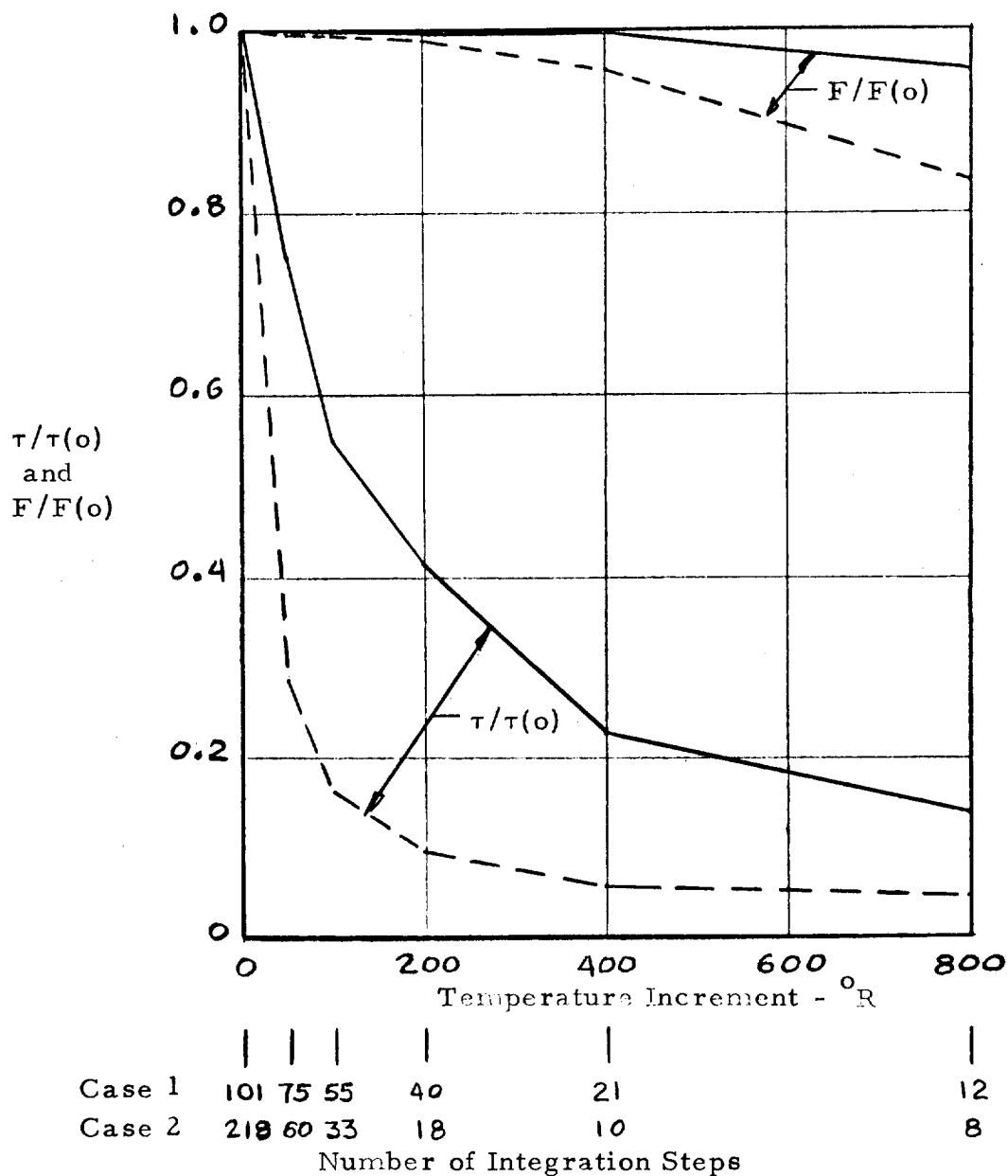


FIGURE 3.4 - Effect of varying temperature step increment on computer running time and calculation accuracy

temperature step criteria will allow the use of a small step size, Δs , which will properly evaluate rapid gradients in the gas flow field. However not enough results have been obtained in different cases to arrive at a criterion for selecting the proper temperature difference.

3.1.3 Wave Number Step Size

The band averaged absorption coefficients and fine structure parameters used for H_2O , CO_2 , and CO in the computer program were obtained from References 6 and 7. In these references the tabulated data are furnished for the wave-number ranges, intervals, and temperatures shown in Table 3.3. Since the water vapor data was used first, the table in the computer program was set-up for the seven temperatures at which water vapor data were furnished using $\Delta\nu = 25 \text{ cm}^{-1}$. When the CO_2 and CO absorption coefficients were added to the program, it was desirable to maintain the same table format and integration step size, so the CO and CO_2 data were interpolated to provide data at the temperatures and wave number interval for which H_2O data existed. This interpolation was performed at MSFC.

In order to check the validity of the interpolation a study was started to evaluate the errors caused by the larger wavenumber increment for CO_2 and to determine if larger increments could be used for all gases to decrease the computer time. However, in the time available, only a few comparisons were completed.

When the CO_2 data were interpolated by MSFC to determine absorption coefficients on 25 wavenumber intervals they actually took the absorption coefficients

TABLE 3.3

Availability of Absorption Coefficient Data

Parameter	Range, cm^{-1}	Interval, cm^{-1}	Temperatures, $^{\circ}\text{K}$									
			300	600	1000	1200	1500	1800	2000	2400	2500	3000
H_2O Absorption Coefficients	50-11000	25	**	**	**	**	**	**	**	**	**	**
CO Absorption Coefficients	1025-2350	25	**	**		**		**		**		**
CO_2 Absorption Coefficients	500-880	5	**	**	**	**	**	**	**	**		**
	1900-2150	10	**	**	**	**	**	**	**	**		**
	2150-2395	5	**	**	**	**	**	**	**	**		**
	3000-3560	10	**	**	**	**	**	**	**	**		**
	3560-3770	5	**	**	**	**	**	**	**	**		**
CO_2 I/d Values	2000-2390	10	**	**		**	**	**		**		**
	3080-3770	10	**	**		**	**	**		**		**

** Indicates data are available at this temperature.

corresponding to multiples of 25 wavenumbers (or linearly interpolated where none were available) rather than averaging the absorption coefficients provided over the new interval. In order to evaluate the accuracy of this procedure and determine the possible errors involved in the use of even larger intervals, a reference computation was made using 10 cm^{-1} intervals, and then runs were made with intervals of 25, 50, and 100 cm^{-1} for comparison. In all the runs, other than those using MSFC data, the absorption coefficients were obtained by averaging the absorption coefficients provided for smaller intervals over the larger interval. The comparison of the results for each wavenumber interval are shown in Figure 3.5. The results indicate that the MSFC interpolated data provide the most accurate results for the particular condition analyzed and that larger intervals than 25 cm^{-1} would lead to excessive errors.

In contrast to the poor results obtained using larger step sizes with CO_2 , the H_2O comparison presented in Figure 3.6 shows very little loss in accuracy in using $\Delta\nu = 100\text{ cm}^{-1}$. These results were obtained using averaged absorption coefficients and looking through a flow field with a linear temperature and isentropic pressure variation from both the hot and the cold sides. If further study substantiates these results, it may be possible to obtain a significant reduction in computation time for rocket plumes from LOX/LH_2 engines.

Notes: $F(\text{REF}) = \text{Reference flux with } \Delta\nu = 10 \text{ cm}^{-1}$
 Flow field temperature = 3000R, pressure =
 750 psfa, CO_2 mole fraction = 0.5,
 path length = 10 inches

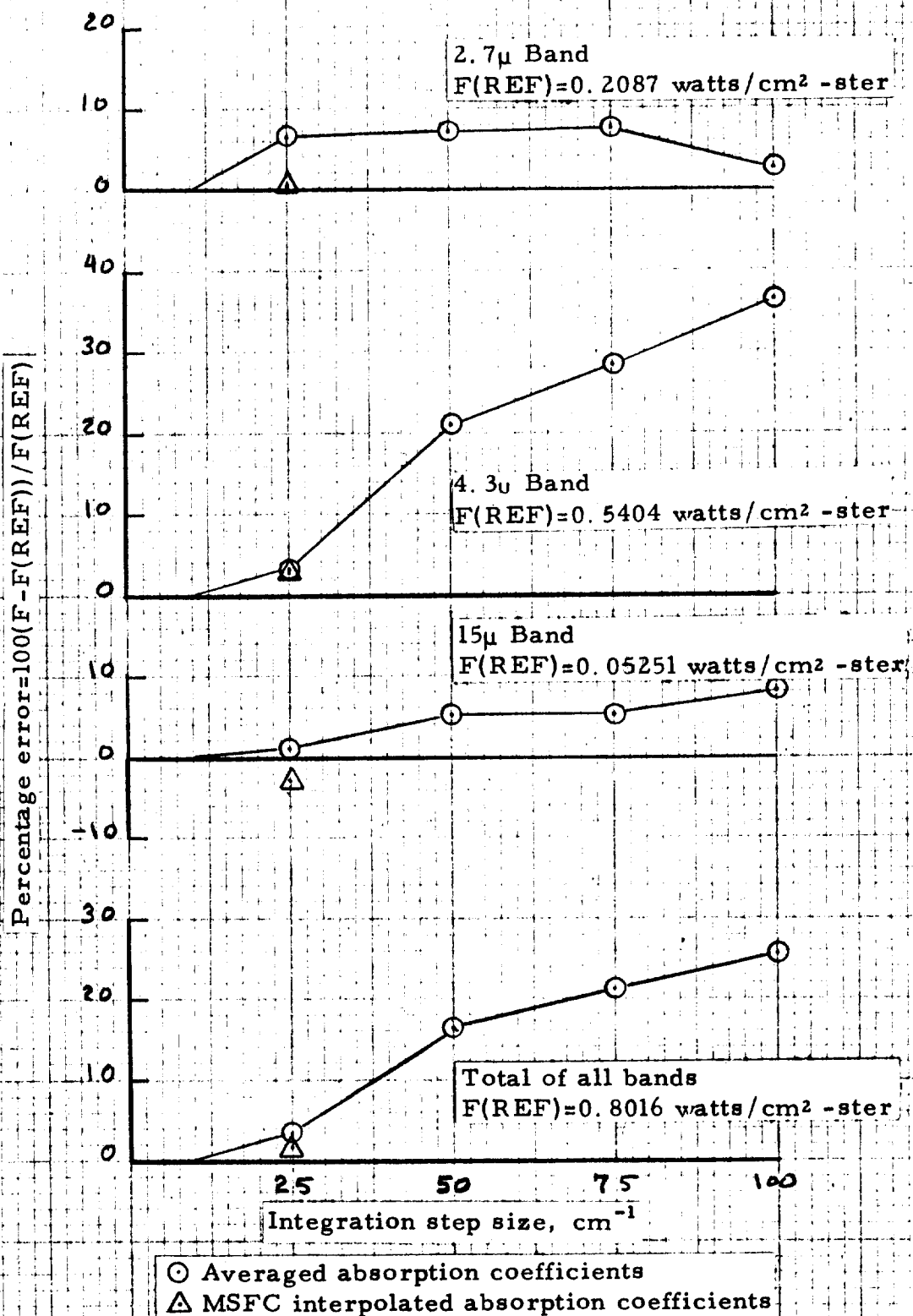


FIGURE 3.5 Effect of wavenumber step size on CO_2 radiation

Notes: $F(\text{REF})$ = reference flux with $\Delta\mu = 25 \text{ cm}^{-1}$ integrated from 50 to 6275 cm^{-1} .
 Flow field has linear temperature variation of 4000 to 2000 °R with a corresponding isentropic pressure variation of 4000 to 110 psfa and a H_2O mole fraction of 0.693. The path length was 36 inches.

- Flow field viewed from the cold side, $F(\text{REF}) = 4.6578 \text{ watts/cm}^2\text{-ster}$
 □ Flow field viewed from the hot side, $F(\text{REF}) = 5.4600 \text{ watts/cm}^2\text{-ster}$

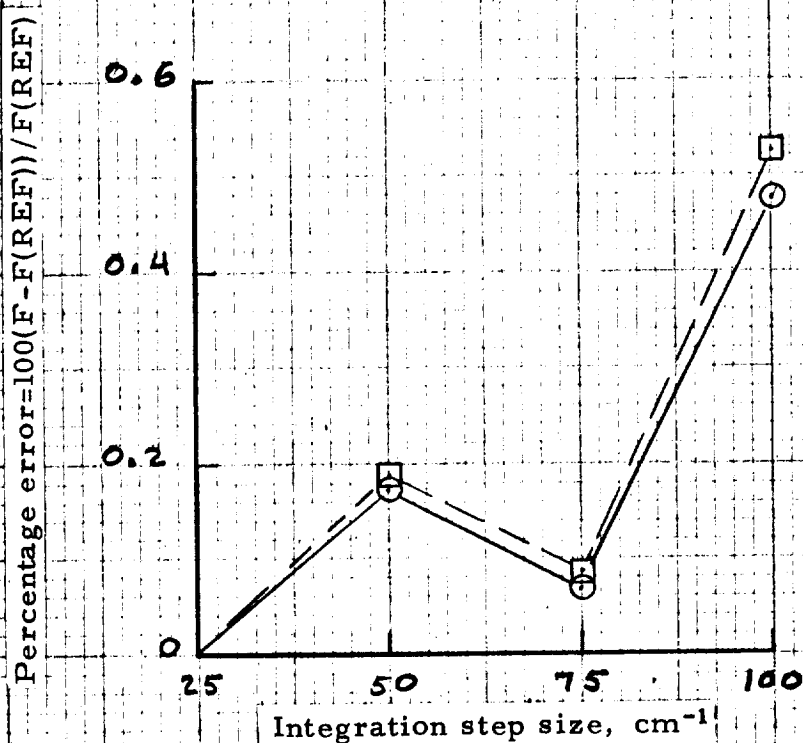


FIGURE 3.6 - Effect of wavenumber step size on H_2O radiation

3.2 Radiation Comparisons

In order to evaluate the MSFC radiation computer program and the absorption coefficient data used in the program, several radiation measurements were made to provide comparative data. These measurements included the J-2 engine spectral measurements described in Section 2.3 and spectral measurements of two short duration model rockets at Cornell Aeronautical Laboratory.

3.2.1 Short Duration Model Tests

The short duration rocket testing technique developed at Cornell Aeronautical Laboratory uses nonsteady flow techniques with gaseous propellants to provide steady flow model rocket firings on the order of 5 to 10 milliseconds. The short test time allows high altitude simulation and eliminates the need for nozzle cooling systems.

Short duration models of two F-1 engines (1/45 scale) and two J-2 engine (1/25 scale) were used in the radiation measurement program. The configuration of the models simulated the engine spacing between the center and outboard engines on the Saturn S-IC and S-II stages. A Warner and Swasey Co. Model 501 fast scanning spectrometer was used for making the spectral measurements. This instrument is capable of making a spectral scan in 1 millisecond with a 0.25 millisecond interval between scans. It uses two detectors and the two channels of output are presented on oscilloscopes and photographed. There is no absolute wavelength reference in the data presentation so that it must be fixed by the spectral features. Therefore, slight wavelength discrepancies in the comparisons to be presented

should be interpreted as uncertainty in the data reduction rather than actual comparative differences.

The radiation measurements were made in the regions indicated in Table 3.4, and comparisons have been made for both the F-1 and J-2 engines at position 1 and for a single F-1 engine at position 5. The spectrometer field of view at the plume used during the tests was approximately 1.6 in. high by 0.25 in. long for the J-2 and 0.8 in. high by 0.25 in. long for the F-1. No comparisons have been made in the impingement region between engines because methods for predicting the three dimensional flow field in this region have not yet been perfected.

The predicted flow field properties and radiation comparisons for the F-1 engine are presented in Figures 3.7 thru 3.10. The comparisons are excellent except for a slight wavelength discrepancy in the long wavelength channel which is attributed to uncertainty in the data reduction procedure described previously.

In contrast to the excellent comparison on the Model F-1 engine, the radiation comparison on the Model J-2 engine shown in Figure 3.11 is very poor. Since the $2.7\mu \text{ H}_2\text{O/CO}_2$ band radiation was in good agreement on both the F-1 measurements, it is unlikely that the disagreement is due to faulty data in the radiation computer program. Therefore, the disagreement is probably caused by poor model operation which was encountered throughout the Model J-2 tests.

3.2.2 J-2 Engine Sea Level Firing

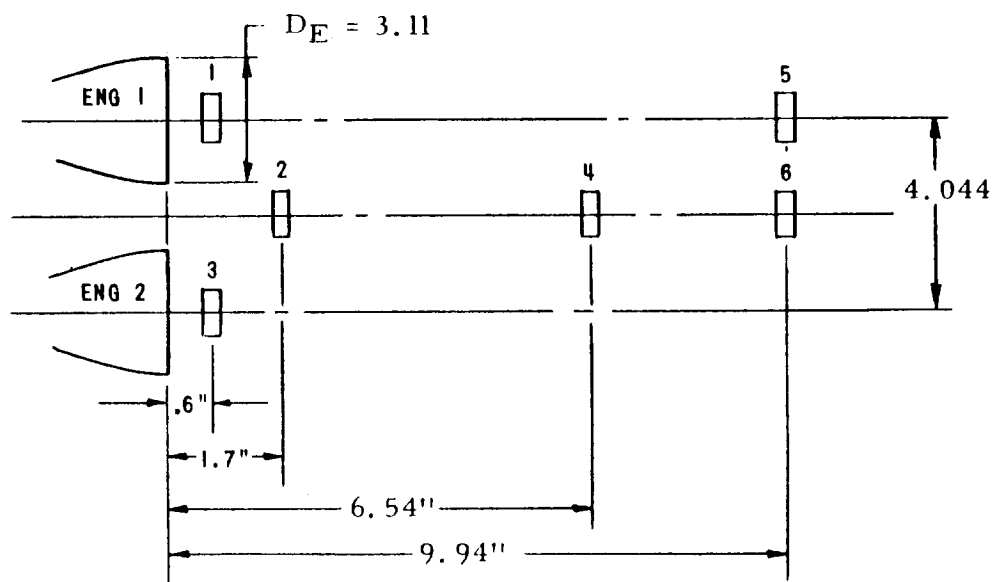
A radiation comparison was made using the spectral data measured in the H_2O bands on a J-2 static sea level firing described in Section 2.3. Due to the complex flow

TABLE 3.4
TEST SUMMARY-TWO-ENGINE PLUME RADIATION STUDY

1) F-1 ENGINE

NOMINAL OPERATING CONDITIONS

ALTITUDE	120,000 FT
COMBUSTION CHAMBER PRESSURE	1000 PSIA
MIXTURE RATIO	$O/F = 2.25 (O_2 / C_2 H_4)$
MEASUREMENT POSITION	1
NO. OF ENGINES OPERATING	2

OBJECTIVE/CONDITIONS

INVESTIGATION OF INSTRUMENT CAPABILITY

SHAKEDOWN AND DEMONSTRATE CAPABILITY
WITH MAXIMUM FIELD OF VIEW (FOV)
AND SLIT SIZE.

MASK TOP AND BOTTOM OF FOV TO DEMONSTRATE
MINIMUM HEIGHT FOV.


REDUCE SLIT WIDTH AND DEMONSTRATE MAXIMUM
SPECTRAL RESOLUTION.

REMARKS

COMPLETED



TABLE 3.4 (Cont.)

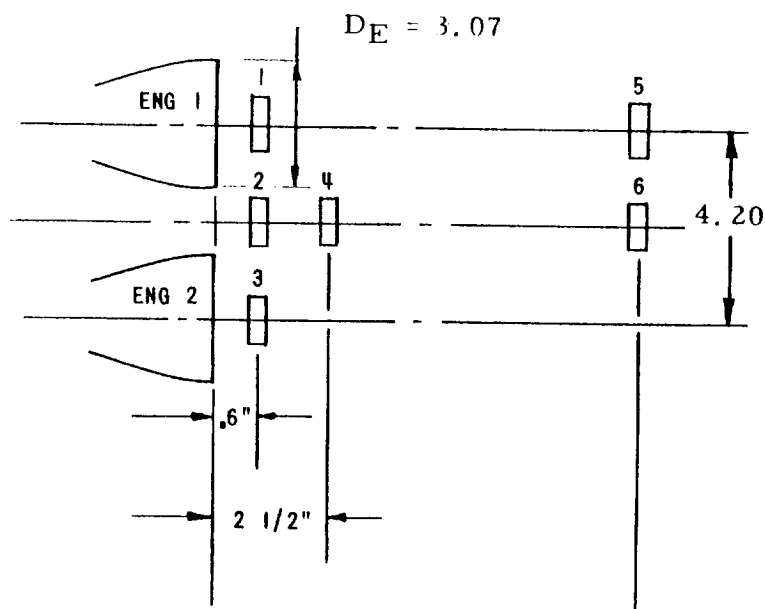
<u>OBJECTIVE/CONDITIONS</u>	<u>REMARKS</u>
EFFECT OF CHAMBER PRESSURE (USING MINIMUM SLIT WIDTH)	COMPLETED
CHAMBER PRESSURE = 600 PSIA WITH ALTITUDE INCREASED FOR CONSTANT P_c/P_∞	
EFFECT OF MIXTURE RATIO (USING MINIMUM SLIT WIDTH)	COMPLETED
$O/F = 2.0$ (OR MINIMUM POSSIBLE WITH SATISFACTORY MODEL PERFORMANCE)	$1.5 \leq O/F \leq 3.0$
$O/F = 3.0$	
PLUME SURVEY (USING MINIMUM FIELD OF VIEW)	COMPLETED
POSITION 3	
POSITION 2	
POSITION 4	
POSITION 5	
POSITION 6	
PLUME SURVEY - SINGLE (NO. 1) ENGINE OPERATION (USING MINIMUM FIELD OF VIEW)	
POSITION 2	
POSITION 4	
POSITION 5	
POSITION 6	

2) J-2 ENGINE

NOMINAL OPERATING CONDITIONS

ALTITUDE	240,000 FT
COMBUSTION CHAMBER PRESSURE	715 PSIA
MIXTURE RATIO	$O/F = 5.5$ (O_2 / H_2)
MEASUREMENT POSITION	1
N° OF ENGINES OPERATING	2

TABLE 3.4 (Cont.)

OBJECTIVE/CONDITIONSREMARKS

INVESTIGATION OF INSTRUMENT CAPABILITY

COMPLETED

SHAKEDOWN AND DEMONSTRATE CAPABILITY WITH
MAXIMUM FIELD OF VIEW (FOV) AND SLIT SIZE.

MASK TOP AND BOTTOM OF FOV TO DEMONSTRATE
MINIMUM HEIGHT FOV.

REDUCE SLIT WIDTH AND DEMONSTRATE MAXIMUM
SPECTRAL RESOLUTION.

EFFECT OF CHAMBER PRESSURE (USING MINIMUM
SLIT WIDTH)

CHAMBER PRESSURE = 1000 PSIA WITH ALTITUDE
DECREASE FOR CONSTANT P_c/P_∞

CHAMBER PRESSURE = 400 PSIA WITH ALTITUDE
INCREASE FOR CONSTANT P_c/P_∞



NOT TESTED

EFFECT OF MIXTURE RATIO (USING MINIMUM
SLIT WIDTH)

O/F = 4.0

COMPLETED

TABLE 3.4 (Cont.)

<u>OBJECTIVE/CONDITIONS</u>		<u>REMARKS</u>
PLUME SURVEY (USING MINIMUM FIELD OF VIEW)		COMPLETED
POSITION 3		
POSITION 2		
POSITION 4		
POSITION 5		
POSITION 6		
PLUME SURVEY - SINGLE (NO. 1) ENGINE OPERATION (USING MINIMUM FIELD OF VIEW)		COMPLETED
POSITION 2		NOT TESTED 
POSITION 4		
POSITION 5		
POSITION 6		

Properties predicted for O_2/C_2H_4 propellants, $O/F=2.25$, $P_c=1000$ psia, $P_{oo}=9.61$ psfa, and equilibrium composition during expansion.

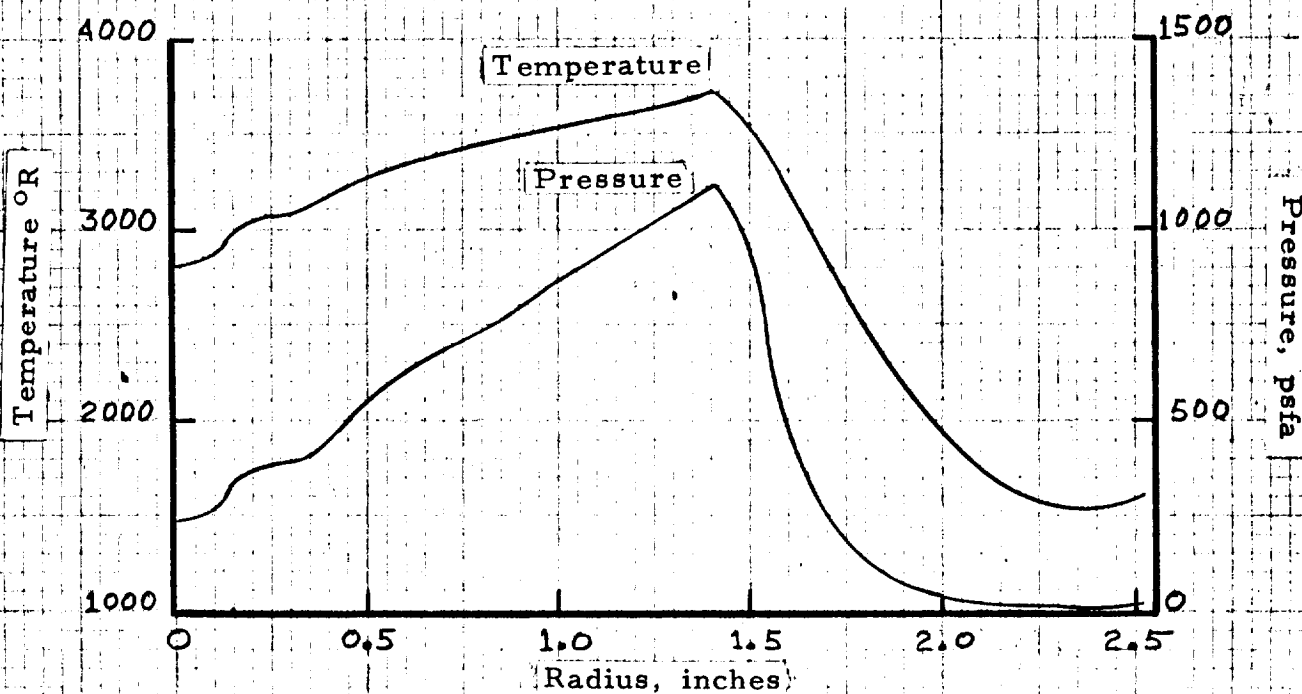
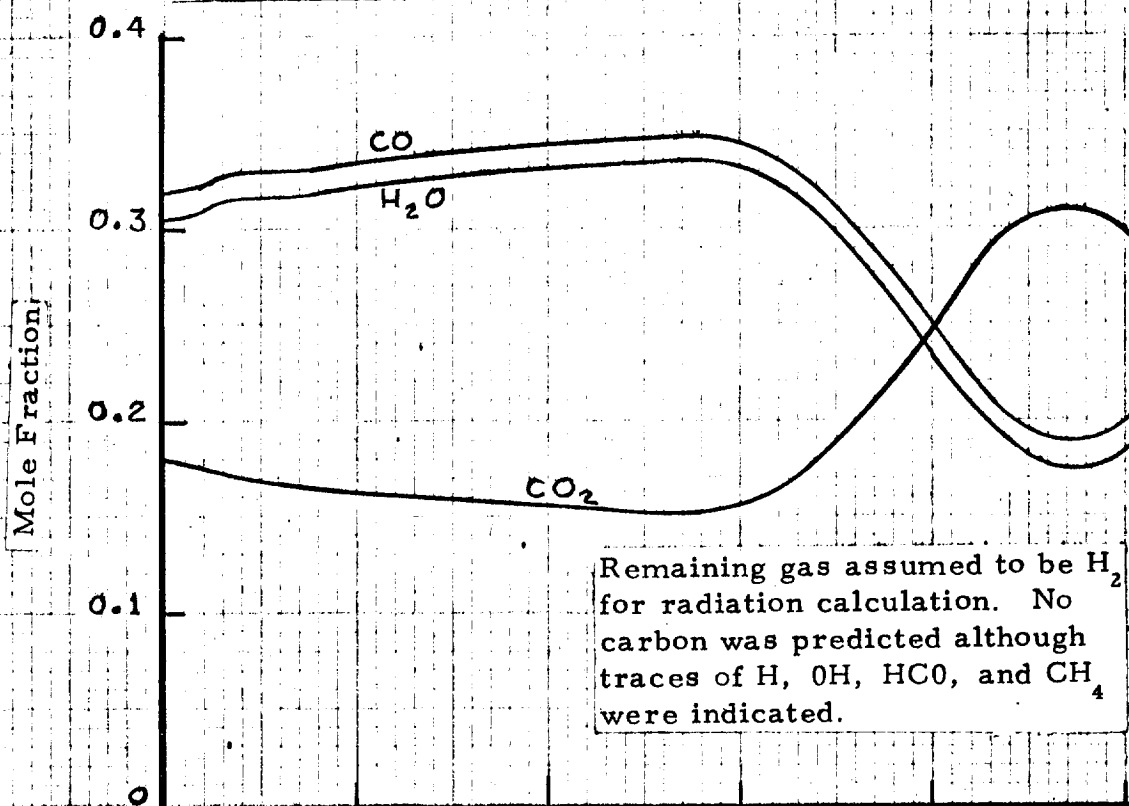


FIGURE 3.7 - Predicted property variations 0.6 in. downstream of a 1/45 scale F-1 engine exit.

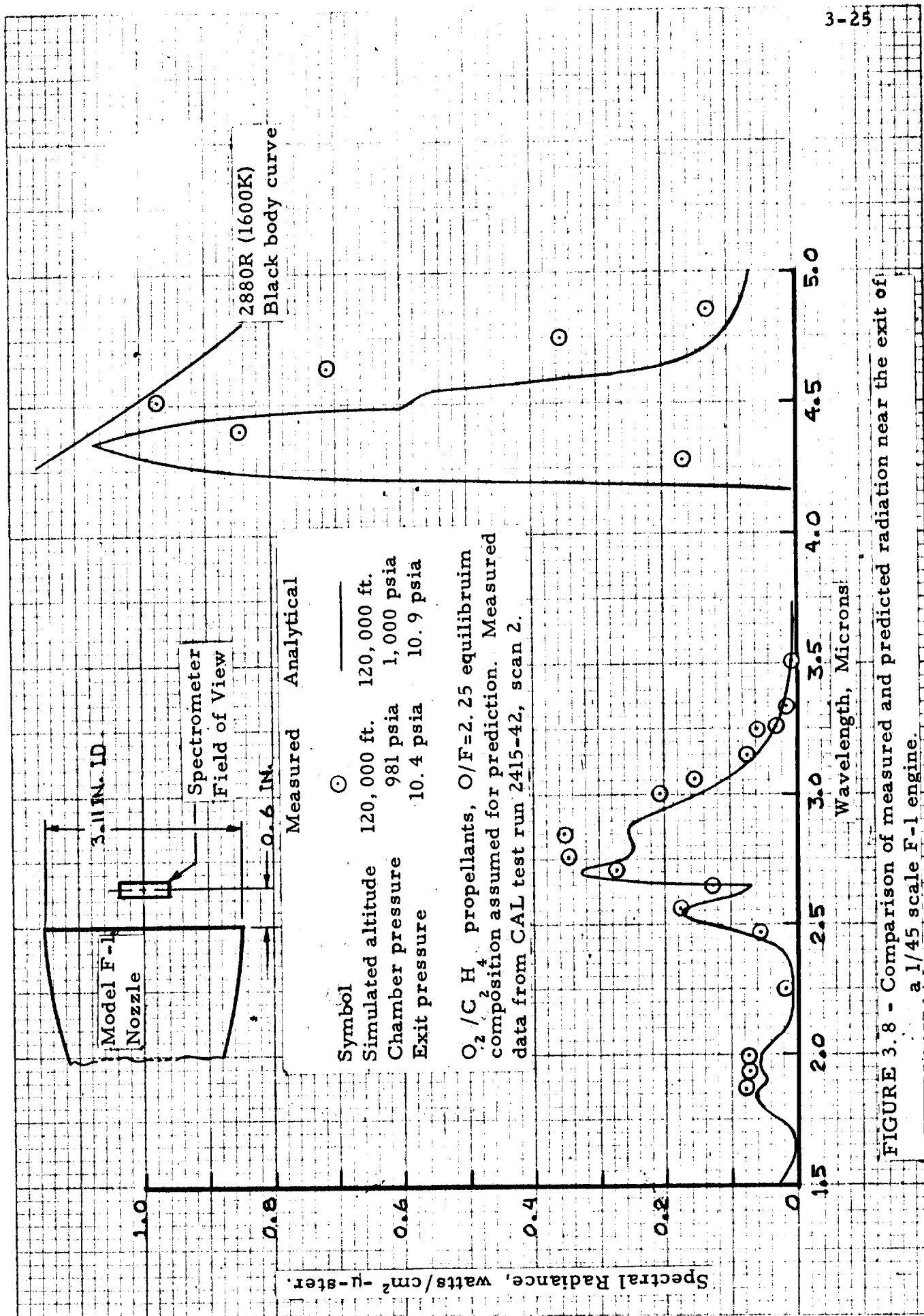


FIGURE 3.8 - Comparison of measured and predicted radiation near the exit of a 1/45 scale F-1 engine.

Properties predicted for O_2/C_2H_4 propellants, $O/F=2.25$, $P_c=1000$ psia, $P_{oo}=9.61$ psfa, and equilibrium composition during expansion.

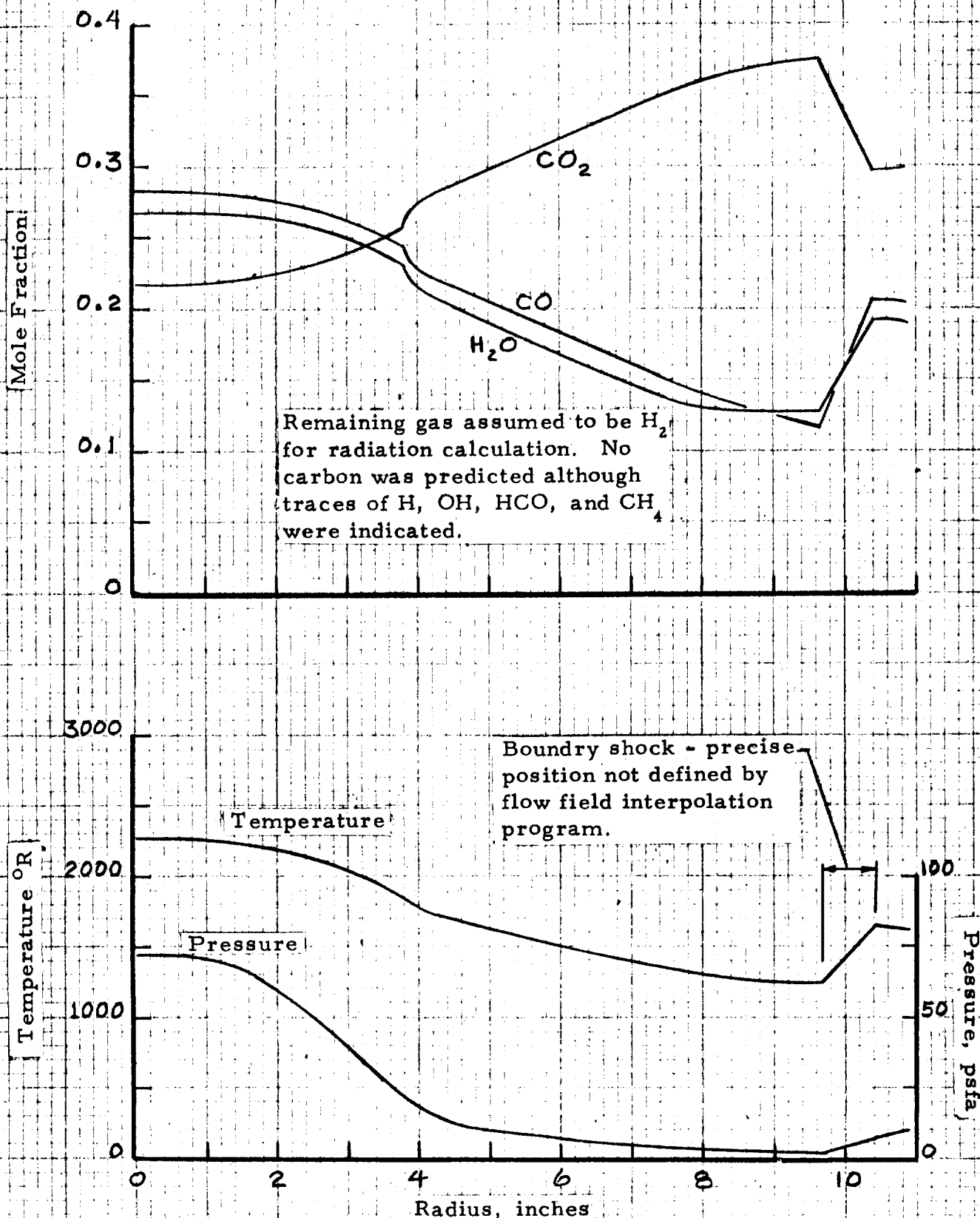


FIGURE 3.9 - Predicted property variations 9.94 in. downstream of a 1/45 scale F-1 engine exit.

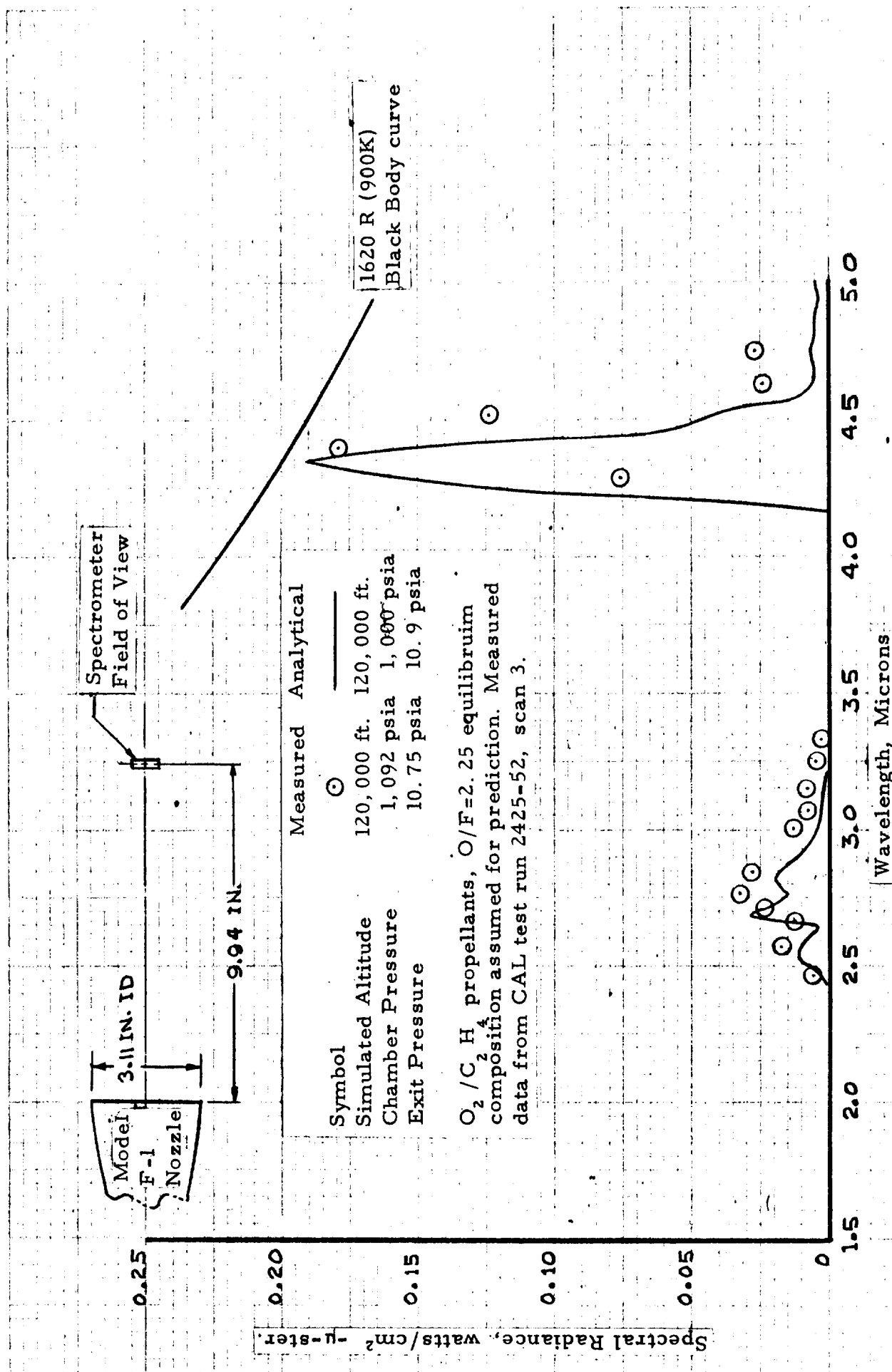
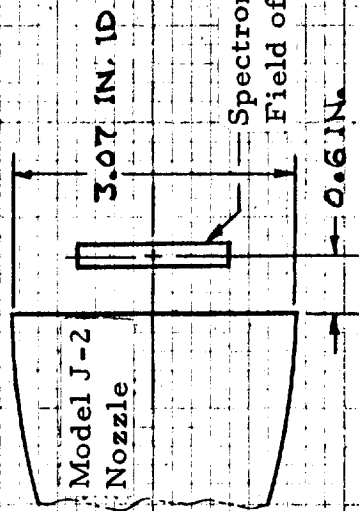


FIGURE 3.10 - Comparison of measured and predicted radiation 9.94 in. aft of the exit of a 1/45 scale F-1 engine.

Simulated altitude = 240,000 ft.
 O_2/H_2 propellants, $O/F \approx 5.5$.
 Equilibrium composition assumed for prediction



— Predicted radiation
 ○ Measured radiation on
 CAL run 2392-19, Scan 4.

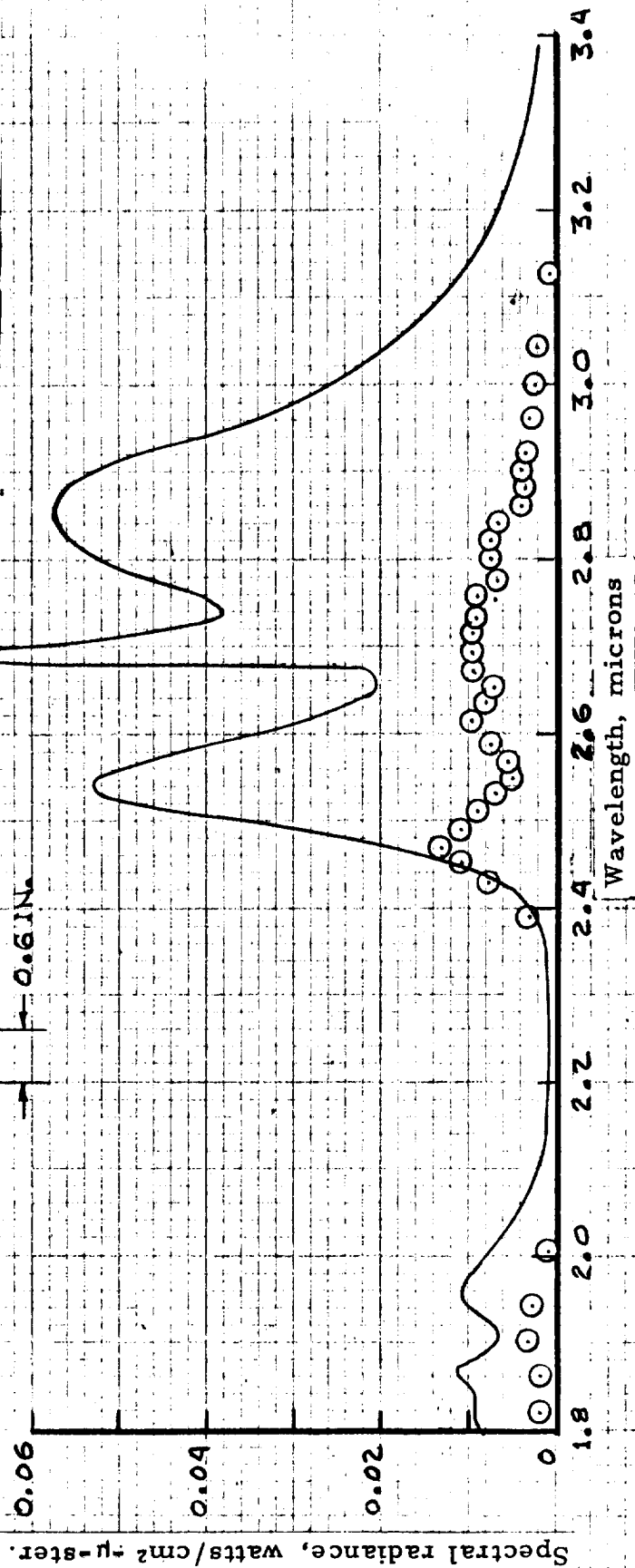


FIGURE 3.11 - Comparison of measured and predicted radiation near the exit of a 1/25 scale J-2 engine.

field on this firing, the predicted plume properties presented in Figure 3.12 are only an approximation. The properties were predicted using equilibrium gas composition in a method of characteristics program. This method does not account for the film cooling water introduced in the diffuser, or the boundary layer which includes turbopump exhaust gases injected into the nozzle. In addition, the nonuniform mixture ratio which probably occurs across the injector face cannot be taken into account.

In view of the uncertainties involved, the comparison of the predicted and measured radiation presented in Figure 3.13 is not too bad, but it certainly fails to verify the accuracy of the prediction techniques. It should be noted that it has not been possible to obtain a post test calibration of the spectrometer used in this measurement, and similar measurements made at other facilities have indicated somewhat lower radiation levels. Until this calibration uncertainty can be resolved it will not be possible to accurately evaluate the flow field and radiation prediction techniques used in this comparison.

3.3 Saturn S-II Base Environment

The base environment of the Saturn S-II stage was determined using base heating tests to specify the convective heating and analytical predictions to estimate the radiation heating.

Base heating model tests of the S-II were conducted from 1962 thru 1965 at both Cornell Aeronautical Laboratory and the MSFC Impulse Base Flow Facility. The results of these tests have been evaluated under this contract and previous

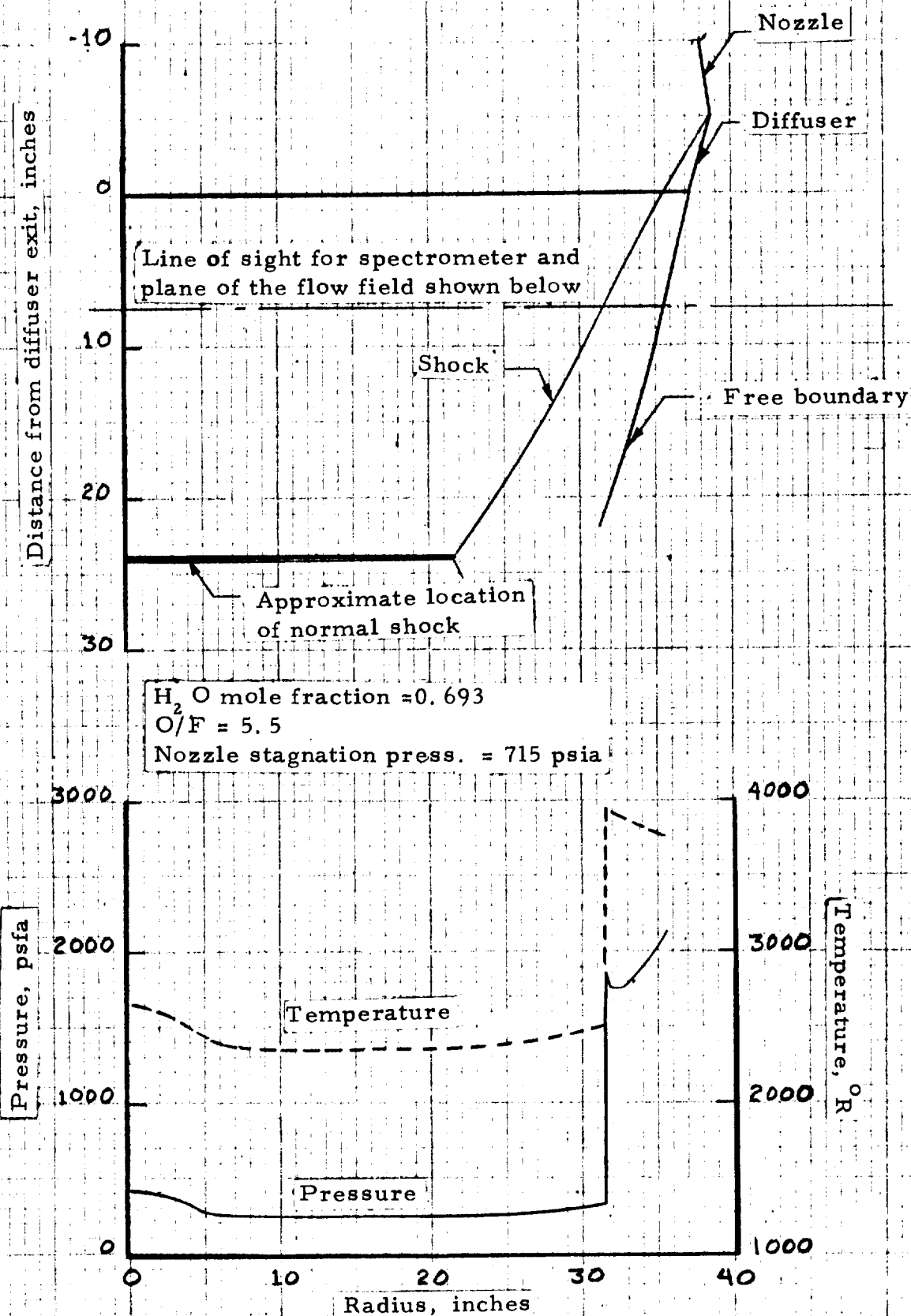


FIGURE 3.12 - Predicted flow field for J-2 sea level firing

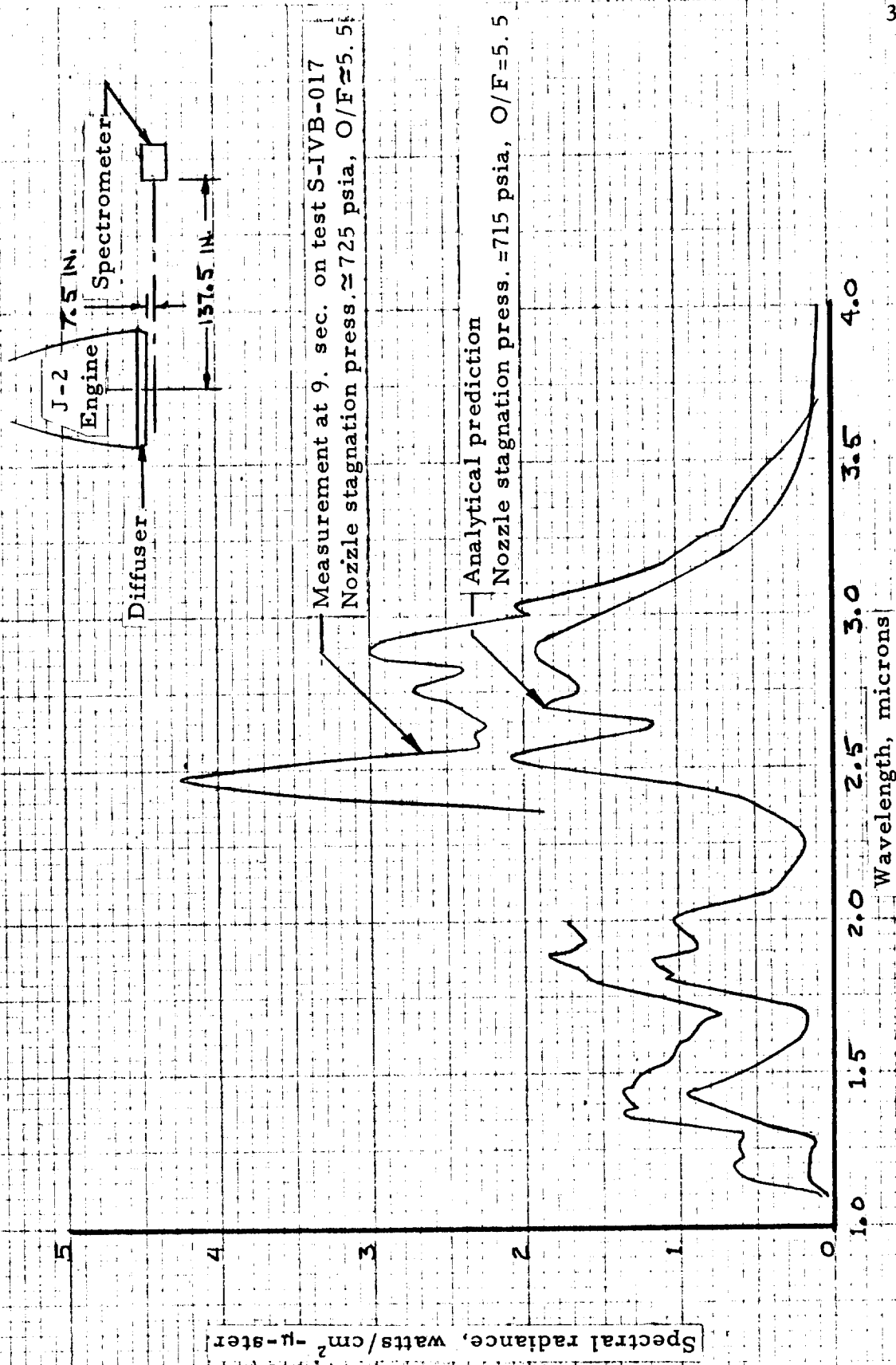


FIGURE 3.13 - Comparison of measured and predicted radiation on a J-2 engine sea level static firing.

contracts, and memorandums have been prepared as required to define environmental conditions.

It is the responsibility of stage contractor (NAA/S&ID) to specify the base thermal environment and this environment must then be approved by the thermal environment branch (R-AERO-AT) at MSFC. S&ID furnished the final design environment for the S-II stage in July 1965. It was reviewed under this contract to assure that it was consistent with the model test results, and its approval was recommended with minor changes as presented in Reference 9. After Reference 9 was prepared, model tests were conducted which indicated that the heating rates on the engine nozzles could be much greater under some conditions than those which had been specified. Since Rocketdyne rather than S&ID had been given the responsibility for the thermal protection of the engines, S&ID was not required to change the environment they had previously published. Therefore, a new environment was published by MSFC based on the evaluation of test results performed under this contract. The most urgent requirement was for a new environment for the center engine, and this was presented in Reference 10. Later, a more complete environment containing possible failure conditions was presented in References 11 and 12.

The S-II base heating tests have been completed and no changes to the convective base environment is anticipated unless the design operating conditions are changed.

The radiation heating rates for the S-II base region were determined by analytical methods at S&ID and appear to be reasonable. However, the MSFC radiation computer program which is now available is theoretically more exact than the methods

used by S&ID, and it would be desirable to make new estimates of radiation at critical locations using the MSFC program.

3.4 Model Flow Nozzle Analysis

Short duration base heating models use a propellant supply system illustrated schematically in Figure 3.14. A steady supply pressure at the flow metering nozzle exists during the time required for the expansion wave to travel the length of the supply tube and return, so steady flow will occur to the model combustion chamber during this time. In order to accurately size the flow metering nozzles, computer programs using real gas equations of state were prepared to calculate the property changes across the unsteady expansion wave and into the nozzle throat.

The gases of primary interest for liquid propellant simulation in base heating models are ethylene (C_2H_4 , simulates RP-1 fuel), oxygen, and hydrogen, but the methods of calculation developed using two different forms of equations of state make them applicable to other gases such as nitrogen, argon, xenon, and several light hydrocarbons.

The computer solution was developed in two parts to provide flexibility in applying the solution to other problems. Part I is used to predict the gas properties and velocity after an unsteady isentropic expansion at constant area. The specified boundary conditions are the initial pressure and temperature and the desired weight flow downstream of the expansion wave. Part II of the computer solution is used to predict the weight flow per unit area at the throat of the flow metering nozzle with the upstream pressure, temperature, and velocity, and the

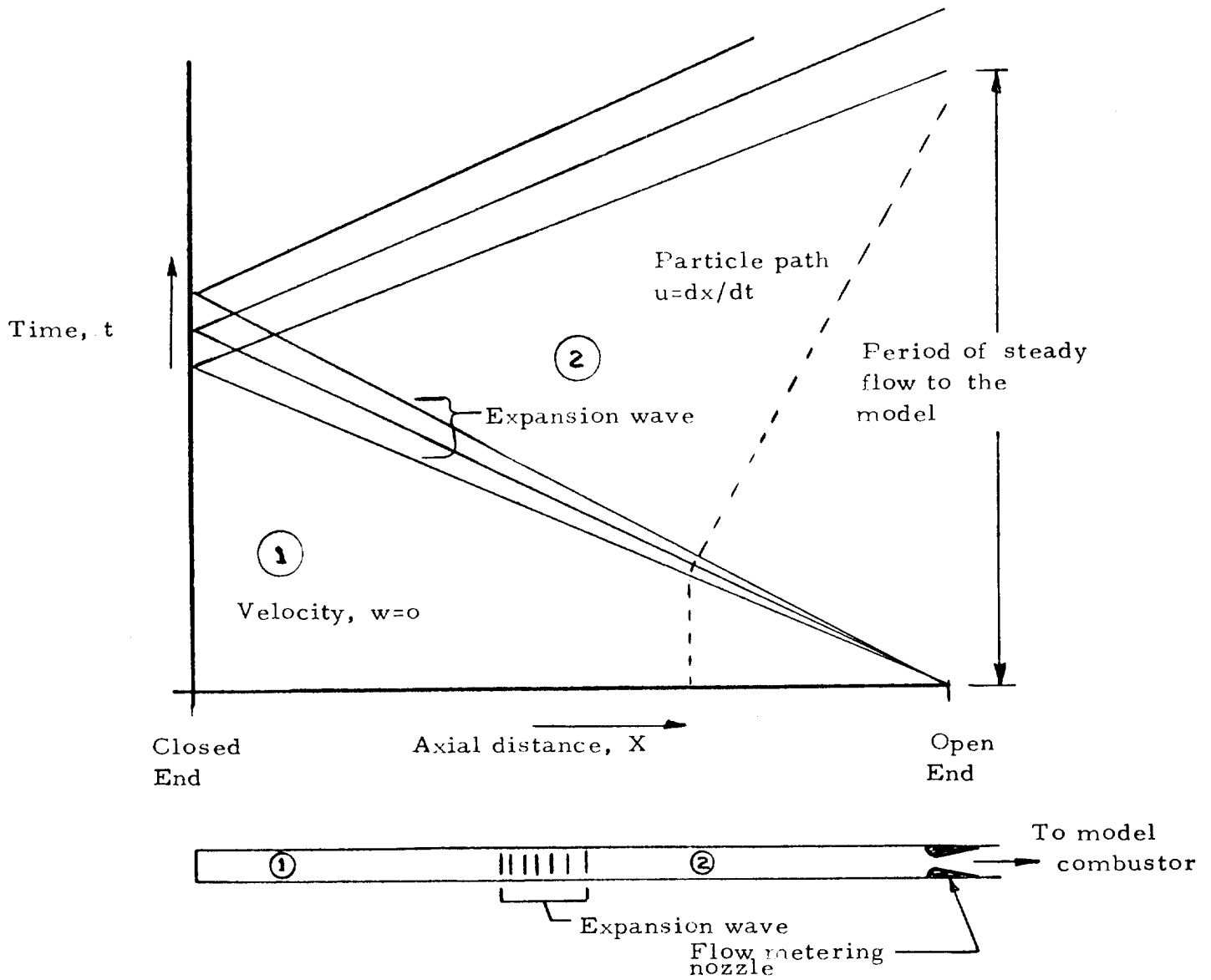


FIGURE 3.14 - Schematic of a short duration model propellant supply system

desired throat Mach number specified. When used for sizing nozzles for base heating models, the output of Part I of the program is used as input to Part II, and the nozzle throat Mach number is taken to be 1. However, Part II of the program could be used for many other applications. In any isentropic steady flow problem it could predict the properties at any point in the flow if the properties and velocity at one point are known.

A complete description of the analysis and computer programs is presented in Reference 8.

4.0 RECOMMENDATIONS

Significant progress has been made in the development of techniques for the prediction of the thermal environment in the base region of rocket vehicles, but additional research is required in several areas. It is recommended that this work should include the following:

1. Further refinement of analytical methods for predicting plume properties to include the effects of turbopump exhaust injection into the nozzle and non-uniform injection in the combustion chamber.
2. Development of methods for predicting plume properties for multi-engine configurations. Finite difference and three-dimensional method of characteristics programs are under development, but have not yet proven satisfactory for highly underexpanded plumes.
3. Additional radiation measurements of full scale engines and clustered model engines operating at simulated high altitude conditions to verify plume and radiation prediction techniques.
4. Base heating model tests with significant scale variations to investigate the effect of scale on the convective heating rate.

5.0 REFERENCES

1. Hughes, A. R. and Reid, J. L., "Radiation Environment of the Saturn V Base Plate, 29 January 1964 to 31 May 1965," Hayes International Corporation, Summary Report, Contract NAS8-11350, ER1155, 25 May 1965.
2. MSFC Memo R-AERO-AT-66-4, "Experimental Determination of Heating Rates and Impingement Pressures from Centaur Retrorocket Exhausts," dated June 28, 1966.
3. Huffaker, R. M., "Radiation from Rocket Exhaust Plumes - Part I: Inhomogeneous Radiant Heat Transfer from Saturn Rocket Exhaust Plumes," AIAA Paper 66-652, June 1966.
4. Conway, L., Yossa, R., and Alligood, B., "Analysis and Computer Program for determining Gaseous Thermal Radiation," Brown Engineering Co. TN R-210, August, 1966.
5. "Study on the Spectral Emissivity of Carbon Particles Produced by a Rocket Motor," Final Report on Contract NAS8-11455, General Dynamics Corp., Convair Division, GD/C-DBE66-006, May, 1966.
6. "Study on Exhaust Plume Radiation Predictions-Interim Progress Report," Contract NAS8-11363, General Dynamics Corp., Convair Division, GD/C-DBE-66-001, January 1966.

7. "Study of Exhaust Plume Radiation Predictions - Interim Progress Report-Part II", Contract NAS8-11363, General Dynamics, Convair Division, GD/C-DBE-66-001a, February, 1966.
8. McKay, G. B. and Reardon, J. E., "The Unsteady and Steady One-Dimensional Expansion of Dense Real Gases," Hayes International Corporation, ER-1332, October 31, 1966.
9. MSFC Memo R-AERO-AT-65-19, "Thermal Design Criteria for the Base Region of the Saturn S-II," dated July 20, 1965.
10. MSFC Memo R-AERO-AT-65-5, "S-II Center Engine Environment," dated September 30, 1965.
11. MSFC Memo R-AERO-AT-66-2, "Thermal Environment for the J-2 Engines on the Saturn S-II," dated June 17, 1966.
12. MSFC Memo R-AERO-47-8-66, "Thermal Environment for an Inoperative Outboard Engine on the Saturn S-II," dated August 26, 1966.